

RESEARCH ARTICLE

Open Access



# PFTK1 kinase regulates axogenesis during development via RhoA activation

Yasmilde Rodríguez González<sup>1</sup>, Fatemeh Kamkar<sup>1^</sup>, Paymaan Jafar-nejad<sup>1,2</sup>, Suzi Wang<sup>1</sup>, Dianbo Qu<sup>1</sup>, Leticia Sanchez Alvarez<sup>1</sup>, Dina Hawari<sup>1</sup>, Margaret Sonnenfeld<sup>1</sup>, Ruth S. Slack<sup>1</sup>, Paul R. Albert<sup>3</sup>, David S. Park<sup>4\*</sup> and Alvin Joselin<sup>4\*</sup>

## Abstract

**Background** PFTK1/Eip63E is a member of the cyclin-dependent kinases (CDKs) family and plays an important role in normal cell cycle progression. Eip63E expresses primarily in postnatal and adult nervous system in *Drosophila melanogaster* but its role in CNS development remains unknown. We sought to understand the function of Eip63E in the CNS by studying the fly ventral nerve cord during development.

**Results** Our results demonstrate that Eip63E regulates axogenesis in neurons and its deficiency leads to neuronal defects. Functional interaction studies performed using the same system identify an interaction between Eip63E and the small GTPase Rho1. Furthermore, deficiency of Eip63E homolog in mice, PFTK1, in a newly generated PFTK1 knockout mice results in increased axonal outgrowth confirming that the developmental defects observed in the fly model are due to defects in axogenesis. Importantly, RhoA phosphorylation and activity are affected by PFTK1 in primary neuronal cultures. We report that GDP-bound inactive RhoA is a substrate of PFTK1 and PFTK1 phosphorylation is required for RhoA activity.

**Conclusions** In conclusion, our work establishes an unreported neuronal role of PFTK1 in axon development mediated by phosphorylation and activation of GDP-bound RhoA. The results presented add to our understanding of the role of Cdk5 in the maintenance of RhoA-mediated axon growth and its impact on CNS development and axonal regeneration.

**Keywords** PFTK1, Eip63E, Rho, Cyclin-dependent kinases, Axogenesis, Neuronal development

<sup>^</sup>Fatemeh Kamkar is deceased.

\*Correspondence:

David S. Park  
david.park1@ucalgary.ca  
Alvin Joselin

Alvin.Joselin1@ucalgary.ca

<sup>1</sup> Department of Cellular and Molecular Medicine, University of Ottawa, Ottawa, ON K1H 8M5, Canada

<sup>2</sup> Present Address: Ionis Pharmaceuticals Inc., Carlsbad, CA 92010, USA

<sup>3</sup> Ottawa Hospital Research Institute and Brain and Mind Research Institute, University of Ottawa, Ottawa, ON K1H 8M5, Canada

<sup>4</sup> Department of Clinical Neurosciences, Hotchkiss Brain Institute, University of Calgary, Calgary, AB T2N 4N1, Canada

## Background

Cyclin-dependent kinases (CDKs) are involved in the regulation of several cellular processes including cell cycle regulation, transcription, translation, and neuronal differentiation and function [1]. Several of these kinases and their interaction partners are typically highly expressed and active in neuronal cells. This includes CDK5, CDK16-18 (PCTAIRE 1–3/ PCTK1-3), and CDK14-15 (PFTAIRE/ PFTK1-2). The best characterized of these CDKs, CDK5, is predominantly active in neurons owing to the tissue-specific expression of its activators, p35/25 and p39. CDK5 deficiency in mice leads to perinatal lethality as a result of defective neuronal



migration, differentiation, and survival. Both PFTK1 and PCTK1 have been shown to be activated by cyclin Y [2, 3]. PFTK1, first identified in *Drosophila melanogaster* (Dmel) [4], and later in mice [5] and humans [6], is highly expressed in the central nervous system (CNS) [7, 8], predominantly in the brain and likely plays an important role in development since PFTAIRE-deficient flies die mostly at early larval stages [9]. Notwithstanding, the function of PFTK1 in CNS development and the downstream substrates PFTK1 regulates has remained largely undiscovered.

In mammals, PFTK exists as 2 separate genes: *PFTAIRE1/PFTK1/CDK14* [6] and *PFTAIRE2/PFTK2/Als2cr7/CDK15* (PubMed Gene ID: 65,061). PFTK1 is highly conserved among different species from yeast to mammals [10]. The fly and worm genome code for the gene known as Eip63-Ecdysone-induced protein 63E which shares 70% homology to mouse PFTK1 [9, 10]. The human *PFTK1* and mouse *Pftk1* are located at (7q21-q22) and (5 A1; 2.61 cM) respectively [5] and show 96% homology. *PFTAIRE2/PFTK2/Als2cr7/CDK15* is recognized in GenBank database and has been reported for its role in conferring resistance to tumor necrosis factor-related apoptosis-inducing ligand (TRAIL) in cancer cells [11]. In the adult mouse, *Pftk1* mRNA is located both in neuroglia and neurons [7, 8] in different regions of the brain such as the cortex, hippocampus, thalamus, cerebellum, and spine. PFTK1 is localized in neuronal cell bodies but not in neurite extensions. During mouse development, *Pftk1* mRNA is expressed at embryonic days 12.5, 15.5, and even 18.5 but soon rises after birth, at P 10.5, and reaches a maximum, comparable to levels in adult mice. This is different from the expression pattern of CDK5 that has a continuous increase from embryonic day 12, followed by a significant increase at birth [7]. All this evidence, together with the knowledge that PFTK1 and CDK5 share a high amino acid sequence similarity (~50–52%), led us to examine the role of PFTK1 during CNS development.

We first examined the role of PFTK1 homolog Eip63E in Dmel ventral nerve cord (VNC) in the regulation of axon and neuronal structure. We show that Eip63E regulates axogenesis in neurons and Eip63E deficiency or downregulation leads to defects in the axon and neuronal structure of the VNC. Furthermore, our functional interaction studies using this model led us to identify Rho1 as an important mediator of Eip63E function. To further confirm this role of PFTK1 in CNS, we describe the characterization of a *Pftk1* knockout (KO) mice. Although no gross abnormalities were observed in morphology, fertility, life span, or anatomical brain structures of the PFTK1 KO mice within the parameters tested, perturbations in axonal growth were observed in cultured

cortical neurons. Corroborating our observations in the flies, overexpression of a dominant negative PFTK1 in WT cultured cortical neurons and primary cortical neurons from *Pftk1* KO mice exhibits faster-growing axons. In line with our observations in the flies, investigations show compelling evidence that PFTK1 phosphorylates GDP-RhoA, and this leads to RhoA activation. These data together point to an important and unexplored role of PFTK1 in axogenesis through its interaction with RhoA implicating PFTK1's role in CNS development.

## Results

### Eip63E-deficient embryos show defasciculation and misguidance of axons in VNC

To examine the role of PFTK1 in CNS development, we used the VNC of Dmel embryos, since it provides an excellent model to study developmental processes [12, 13]. Additionally, flies only have one homolog gene for PFTK (Eip63E) and do not have other neuronal CDKs closely related to PFTK1 that could add a level of complexity, due to possible compensation.

We used two different Eip63E mutant Dmel lines, carrying the *Df(3L)E1* and *Eip63E<sup>81</sup>* alleles respectively [9]. The nature of both these alleles is different in that the former is a result of a large deletion that spans the transcription initiation region to the entire kinase domain of Eip63E and affects two other adjacent genes, namely *SDE3/Armitage* [14] and *1(3)63D* [9]. Alternatively, *Eip63E<sup>81</sup>* is a smaller 48-bp in-frame deletion that removes 16 codons within Eip63E conserved kinase domain (213–228). Since both alleles lead to embryonic lethality, the fly's populations are maintained as heterozygous mutants with the use of balancer chromosomes. Because we wanted to examine embryos, both mutant lines were balanced with a balancer chromosome which expresses GFP from embryonic stages 9–10 to adulthood [15]. Once the expression of GFP kicks in (absent before stage 9), Eip63E-deficient embryos are distinguishable from the rest of the population by the absence of GFP expression.

Initially, BP102 or fasciclin-II (1D4) were both used as different markers to assess the VNC structures of stage 14–15 embryos. Both are expressed in the axon bundles that define the commissural and longitudinal connectives of the fly VNC [16, 17]. Both markers confirmed axonal defects in the Eip63E-deficient embryos for both mutant alleles (Fig. 1). Eip63E-deficient embryos (GFP negative) show a diffuse appearance of the axonal pathways (Fig. 1A and B) suggesting defasciculation of axon bundles. Additionally, axons appear not to follow the appropriate pathways, leading to malformation of the ladder-like normal axonal structure of the VNC, with

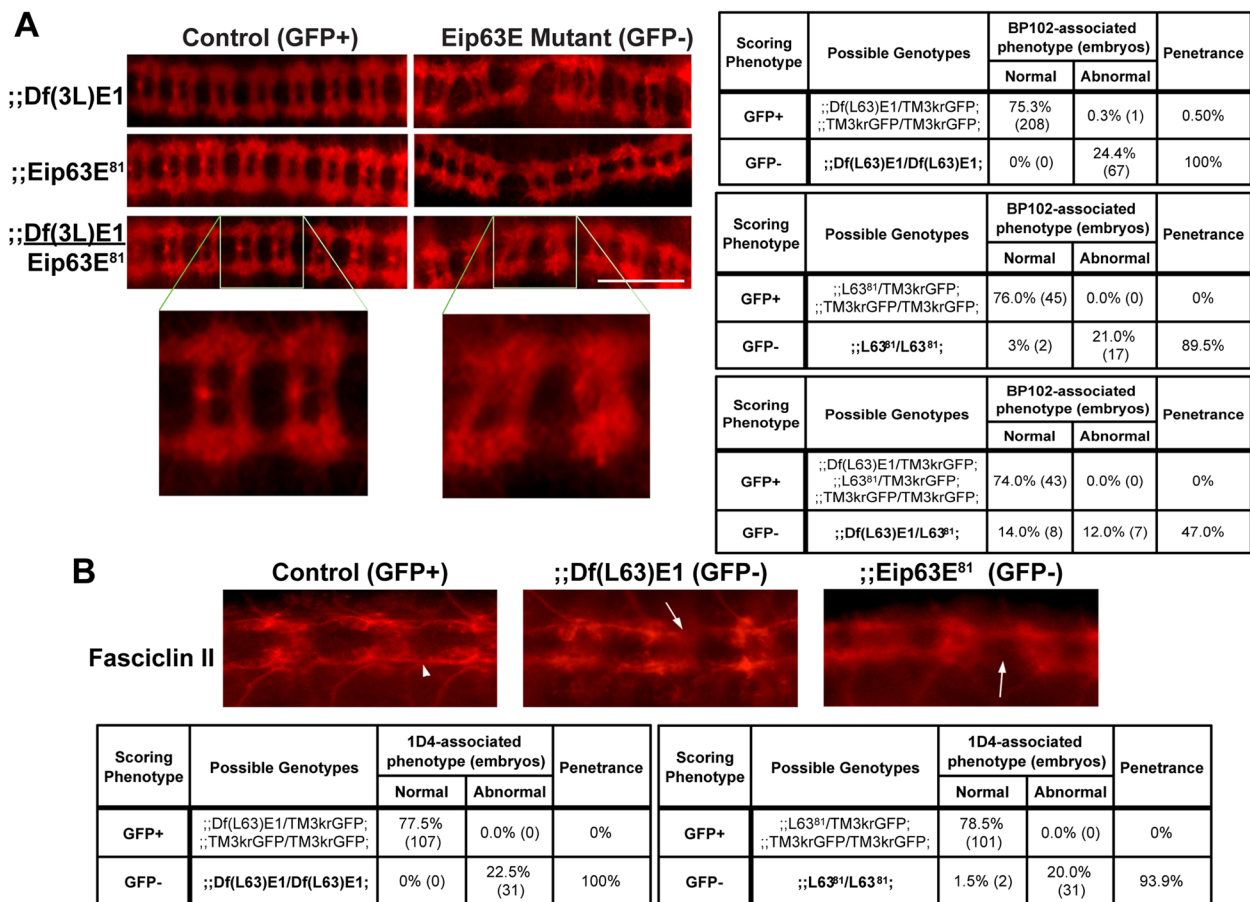


**Fig. 1** Eip63E deficiency leads to defasciculation and misguidance of VNC axons. Ventral views of whole mount stage 14–15 embryos from both Eip63E mutant lines, co-stained for GFP and BP102 (A) or Fasciclin-II (1D4 mAb) (B). Penetrance of VNC defects was calculated as the % of embryos of a given scoring phenotype that show any defect from the total population of such phenotype (GFP + or GFP – embryos). Arrowhead points to normal-looking longitudinal connectives and arrows point to disrupted structures in deficient embryos. L63<sup>81</sup> denotes Eip63E<sup>81</sup>. Scale bar 50 μm

disruption of both commissural and longitudinal pathways (Fig. 1A and B).

Given the difference in genetic background between the mutant alleles, we needed to test if the observed VNC defects were primarily related to Eip63E. We therefore generated trans-heterozygous mutant embryos containing one copy of each of the mutant alleles and stained for BP102. As shown in Fig. 1A (bottom panel) and its corresponding scoring chart (Fig. 1A, bottom right), axonal defects like those of the single deficiencies were observed in the trans-heterozygous mutants. It should also be noted that no defects were ever observed in GFP-positive embryos, suggesting that none of the mutant alleles exhibit dominant-negative behavior. Together, these results suggest that axonal defects were indeed caused, at least in part, by Eip63E deficiency and not only due to background mutations.

**Early neurogenesis events are defective in Eip63E mutants.**

An early event in Dmel CNS development is the formation of the ventral midline. This has an essential impact on axon outgrowth/guidance and the proper ladder-like scaffold of axons of the VNC [17, 18]. To determine if midline defects were primary to the defects observed at stages 14–15, we assessed midline formation in embryos of the Eip63E<sup>81</sup> mutant line as compared to wild-type W<sup>118</sup> embryos. W<sup>118</sup> was needed as control in these studies since we did not have any way to genotype the Eip63E<sup>81</sup> embryos before stage 9 due to the absence of GFP expression before that stage (this also rules out GFP as a source of the defects). We performed immunostaining for single-minded (sim), a protein which is exclusively expressed in midline precursors and their progeny and is a master regulator of the differentiation of midline neurons and glial cells [19]. Eip63E deficiency does not have any apparent effect on midline formation since no defects were found in embryos from the Eip63E<sup>81</sup> line (stages

5–10) compared to WT embryos (Fig. 2A). Furthermore, HRP staining at stage 11 (Fig. 2C, bottom panel) suggests that the ventral midline appears normal in Eip63E-deficient embryos even when the deficiency might lead to axon defects and abnormal HRP staining at later stages.

Another hallmark of the Dmel embryo development is the segmentation of the embryo which is triggered early (within the first 3 h) leading to the formation of stripe-like segments along the anterior–posterior axis. Segment polarity genes are part of the expression cascade that regulate this process and are expressed in 14 stripes at the onset of gastrulation (~3 h, stages 6–7) [20]. These genes, which include engrailed (*en*) and invected (*inv*), are major players in neurogenesis [21, 22]. We examined the expression pattern of *en/inv* proteins to evaluate if

segmentation and/or neuroblast delamination/segregation was affected in Eip63E-deficient embryos. Immunostaining with the 4D9 antibody, which recognizes both *en/inv* proteins, revealed that 18% of stage 8–9 embryos from the Eip63E<sup>81</sup> line show abnormal phenotypes (Fig. 2B). It is likely that embryos with affected segmentation (Fig. 2B, second panel down from the top) do not make it further into development. Interestingly, those that can compensate (stages 10–11) do not show segmentation defects but disorganization and morphological differences of cell bodies within segments. Since genotyping is not practical at these stages, it is not possible to link these phenotypes to Eip63E deficiency. It should be noted that comparable defects were observed in similarly timed embryos from the Df(3L)E1 line (data

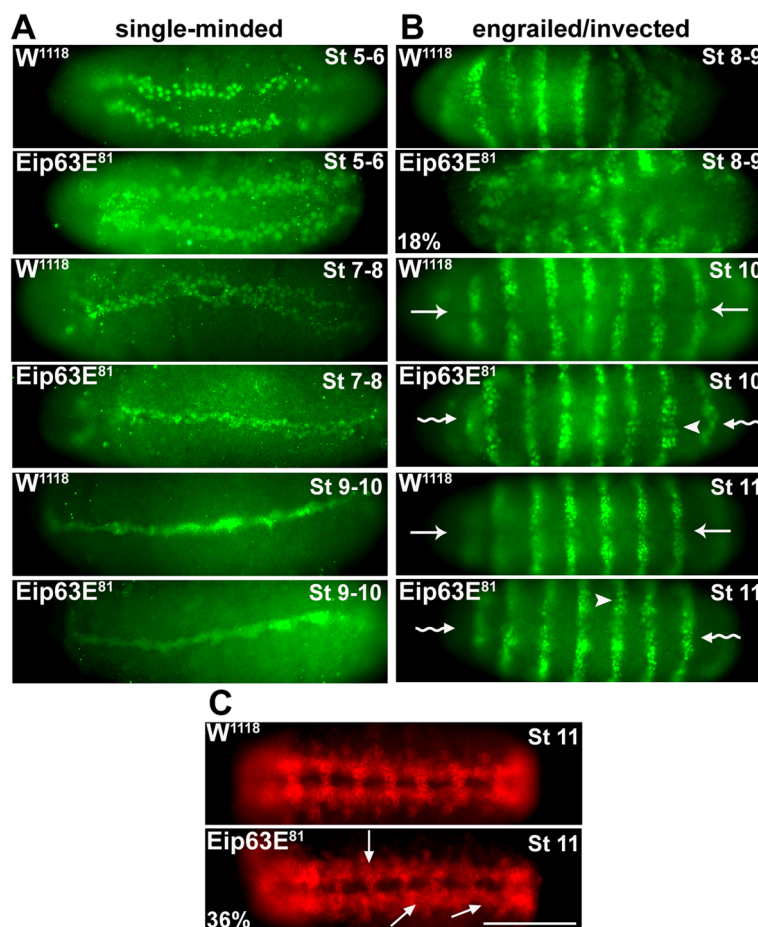


**Fig. 2** Eip63E deficiency leads to early embryonic developmental defects. Ventral views (unless otherwise specified) of whole-mount embryos are shown head to the left. Stage 5–8 embryos are from Eip63E<sup>81</sup> line of unknown genotype. Panels for stages 8–9 onward show Eip63E<sup>81</sup> homozygous mutant embryos. **A** Staining for single-minded at early embryonic stages (st 5–10) shows no gross difference in midline formation but cellular morphological differences are noticeable. **B** Staining for engrailed/ invected (4D9 mAb). 18% ( $n=48$ ) of total population of stage 8–9 embryos show acute segmentation defects. At stages 10–11, cell bodies appear disorganized (arrowheads) to the extent of loss of hemi-segments division at the midline (wavy arrow) compared to control (straight arrow). **C** Staining for the HRP antigen. At late stage 11, precocious axon outgrowth (arrows) seen in 36% of deficient embryos ( $n=52$ ). Scale bar 50 μm

not shown). In comparison, only 3% of WT embryos of similar stages show any defects. Although abnormalities were also observed in older Eip63E-deficient embryos (stages 10), their incidence decreased (8% Eip63E<sup>81</sup>). This is likely due to the adverse effects of the defect on the survival of defective embryos combined with a decreased yield due to treatment methodology for the morphologically defective embryos. Taken together, these results suggest a potential role for Eip63E in the delamination of neuroblasts and/or their segregation.

### Axon outgrowth occurs prematurely in Eip63E-deficient embryos

Axogenesis in Dmel embryos starts at ~7:30 h into development (early stage 12) after specification of the midline cells that will guide the pioneer axons contra-laterally to cross the midline [17, 23]. To elucidate how early in CNS development axon defects start to appear, we examined CNS features using an anti-horseradish peroxidase antibody which recognizes a carbohydrate epitope (called HRP for simplicity) present on several cell-surface molecules expressed by neuronal cell bodies and axons [24] including fasciclin II [25]. Ten percent of stage 8–9 embryos which are mixed population from the Eip63E<sup>81</sup> line ( $n=48$ ) showed premature HRP staining distinct from WT W<sup>118</sup> embryos (Fig. 2C, top 2 panels). Lateral views of the embryos are presented since this abnormality became more evident when looking laterally. Stage 9–10 W<sup>118</sup> embryos show faint, background staining along the ventral region of the embryo where VNC axons would later appear. In contrast, Eip63E<sup>81</sup> embryos show HRP-positive structures at stages 9–10 distinct from W<sup>118</sup> embryos (Fig. 2C, middle 2 panels). By late stage 11, 36% of Eip63E<sup>81</sup>-deficient embryos (GFP<sup>-</sup>,  $n=52$ ) show premature, and in some cases misguided, axon outgrowth affecting several segments of the VNC (Fig. 2C, bottom 2 panels). These embryonic defects although subtle show that axon-related defects appear early in development, from the time axon structures tend to emerge and that the incidence of axon defects in deficient embryos consistently increases.

### Eip63E deficiency leads to other morphological defects in the CNS

To further evaluate the effects of Eip63E deficiency on neuronal cell bodies, we stained for the product of the *elav* (embryonic lethal abnormal visual system) gene which codes for an RNA-binding protein that is expressed exclusively in neurons [26] and is required during the development and maintenance of the CNS [27]. ELAV expression pattern in Eip63E<sup>81</sup>-deficient (GFP<sup>-</sup>) embryos revealed defects as early as stage 12 (Fig. 3A). ELAV staining is diffuse in the

Eip63E-deficient compared to GFP + embryos of similar stages. Additionally, the morphology of neuromeres and hemisegments along the VNC of mutant embryos was disrupted and abnormal, making it difficult to distinguish midline neurons from the rest in several VNC segments of stage 12–13 Eip63E-deficient embryos (Fig. 3A).

Neuronal abnormalities were observed using neuronal marker, Neuroglian (long isoform, BP-104), a cell-adhesion molecule expressed in a sub-population of neuronal cell bodies and axons [28]. Malformation of neuromeres and hemisegments linked to axon pathfinding defects are observed in Eip63E<sup>81</sup>-deficient embryos (Fig. 3B). The lack of symmetry between the hemisegments and the midline pattern of different neuromeres suggest a disorganization of neuronal cell bodies consistent with the observations for *elav* immunostaining. Disarray of neurons and axons was also observed when VNC flat preparations of timed stage 11 embryos were co-stained for Futsch and anti-HRP (Fig. 3F). Futsch is a microtubule-associated protein, necessary for axon and dendrite development in *Drosophila* [29]. The axonal bundles in Eip63E deficiency (both Df(3L)E1 and Eip63E<sup>81</sup> alleles) appear defasciculated when compared with controls (HRP staining) and defective hemisegments coincide with misplaced neurons (Futsch staining).

As in vertebrates, glial cells play a key role in neuronal development in Dmel, particularly in axon guidance [30–32]. Since the axon defects linked to Eip63E deficiency appear early in CNS development, we explored the effect of the deficiency on glial cells. The reverse-polarity (*Repo*) gene codes for a homeodomain protein that is expressed in all embryonic glial populations, except midline glial cells, from stage 9 glioblasts to mature glial cells [33]. Co-staining of glial cells using *Repo* and of axons using HRP antibody (Fig. 3D) revealed disorganization of glial cell bodies in Eip63E<sup>81</sup>-deficient embryos when compared to controls. Interestingly, those defects were much more severe (even with a smaller cell population) for the Df(3L)E1-deficient embryos (data not shown).

When we combined the penetrance associated with all these relevant neuronal and axonal markers along the VNC structures (Additional file 1: Fig. S1), it became apparent that Df(3L)E1 allele-associated defects appear later in development with more severe outcomes (higher penetrance) than those associated with Eip63E<sup>81</sup> allele. For both mutant alleles, axon defects were also accompanied by defects in neuronal cell body localization. This pointed to the possibility that axonal defects could be caused by the mis-localization of neurons rather than a neuronal Eip63E requirement.

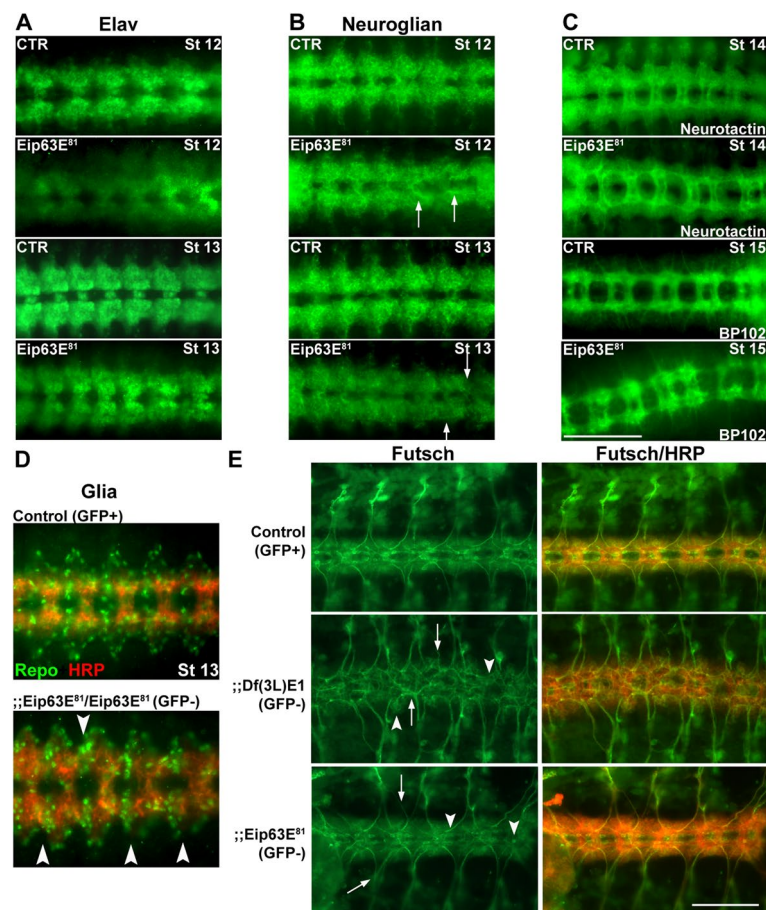


**Fig. 3** Eip63E deficiency leads to early segmentation defects. **A–D** Ventral views of whole-mount embryos stages 12–15 shown head to the left. CTR show GFP + embryos (wild-type and mutant heterozygous population) and Eip63E<sup>B1</sup> represent homozygous mutant embryos (GFP–). Immunostaining for Neuroglian (**B**), Neurotactin (**C**, top 2 panels), and BP102 (**C**, bottom 2 panels) showing axon defects (arrows). **D** Co-staining for glial populations (Repo) and axons (HRP) showing disorganized cell bodies (arrowheads). **E** VNC flat preparations of timed embryos (10–11 h, stage 14) co-stained for Futsch and HRP are shown dorsal up, head to the left. Arrowheads point to some of the structures where neuronal organization is different from control embryos. Arrows point to examples of axon growth abnormalities. Scale bar 50  $\mu$ m

### Specific downregulation of Eip63E in neurons leads to axon defects

To further confirm that the axonal defects observed in the Eip63E mutants were indeed due to Eip63E deficiency during CNS development and rule out any background effects of the germ-line deletion, we performed tissue-time-specific downregulation of Eip63E using the Gal4-UAS system [34]. Utilizing the UAS-RNAi fly lines for Eip63E developed by the Vienna Drosophila RNAi Centre, Eip63E was knocked down (KD) using drivers for all cells (ubiquitous expression, Act5-Gal4), neurons (elav-Gal4), glia (repo-Gal4), mesoderm/visceral muscles (mef2-Gal4), dorsal epidermis/ peripheral nervous system (PNS) (GawB109.69-Gal4), and digestive system/ longitudinal muscles (GawBtey5053A-Gal4) (Fig. 4). The Krüppel-GFP balancers used before would not be appropriate for these experiments, since they possess an

internal Gal4-UAS system to regulate GFP expression that would interfere with our experiments. Therefore, lines were introduced to balancer chromosomes expressing ACT5-GFP instead, which provided for GFP expression under the Actin A5c promoter [35]. Nevertheless, the fluorescent labels for these alternative balancers had weak expression at embryonic stages, even when amplified with anti-GFP staining, making it difficult to genotype the embryos. Therefore, the results are reported as % of defects relative to the total embryonic population.

As shown in Fig. 4, ubiquitous downregulation of Eip63E resulted in axon defects and lethality similar to those observed with the germline-deficient lines. Half of the embryonic population was expected to be control (no driver). Axon defects were observed in 59.7% of the embryonic population (Fig. 4B). This would suggest a 100% penetrance of defects for ubiquitous

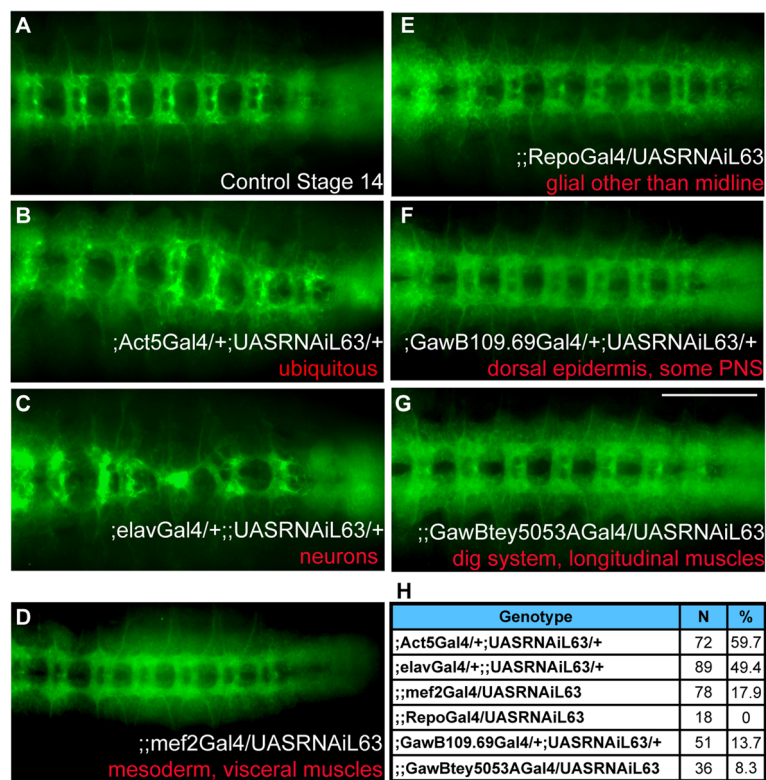


**Fig. 4** Only ubiquitous and neuronal downregulation of Eip63E leads to embryonic axon defects. Ventral views of stage 14 whole-mount embryos stained with BP102 shown head to the left. A UAS-Gal4 approach was used to drive Eip63E downregulation in specific tissues during embryonic development. Embryos negative for GFP (present in balancers for both the Gal4 and the UAS lines) were considered experimental embryos vs the GFP positive of the same progeny. **A** A representative GFP+ embryo is shown. **B** Ubiquitous downregulation led to a replica of the germline deficiency lines, with regards to CNS defective phenotype and developmental lethality (see text for details). **C** Neuronal-specific downregulation led to a robust and highly penetrant axonal phenotype. **D–G** Downregulation of Eip63E in other tested tissue (indicated in red) did not cause any detectable axonal defects. The number of embryos per genotype and the percentage of embryos per group showing axonal defects is summarized in **H**. Scale bar 50  $\mu$ m

downregulation. Additionally, when embryos were left to complete the life cycle, all the flies that eclosed were positive for the balancer phenotypic marker, suggesting that (like the germ-line mutants) ubiquitous downregulation of Eip63E is developmentally lethal and corroborating the effectiveness of the RNAi construct used.

When Eip63E was specifically downregulated in neurons using the neuron-specific elav-Gal4 driver (Fig. 4C), VNC defects were observed in 49.4% of the embryonic population. Since half the embryonic population is expected to be driver only without UAS-RNAi expression, these results suggest close to 100% penetrance of defects upon neuronal downregulation. These results are consistent with the notion that neuronal Eip63E function is required for axon development in *Dmel*. Intriguingly, when development was not interrupted for embryo collection, we observed an equivalent number of Cyo-positive and Cyo-negative flies eclosing ( $n=72$  vs  $n=76$ ). This suggests that although important in CNS development, Eip63E neuronal

function alone does not play a role in developmental survival.

No noticeable defects were observed when Eip63E was specifically knocked down in glial, or any of the other tissues (Fig. 4D to G). The total number of embryos per group and the percentage of embryos with observed axon defects are presented in Fig. 4H. These results suggest that the functions of Eip63E in neurons, and possibly neuroblasts, are key to axon development in *Drosophila*, especially for the regulation of axon outgrowth and guidance.

#### **Drosophila Eip63E functionally interacts with Rho1**

Previous reports have shown that CDK5 and PCTAIREs regulate axon development by functionally interacting with the Rho family of GTPases [36–38]. However, whether such an interaction exists between PFTK1/Eip63E and Rho GTPases is not known. We used the *Dmel* line expressing the dominant-negative Rho1<sup>72F</sup> allele [39], to explore this possibility. Homozygosity for

the  $Rho1^{72F}$  mutant allele leads to 100% lethality and this germline was therefore maintained as a balanced heterozygous population. When we characterized the embryonic population staining for BP102 marker, we detected that 97% of homozygous mutant embryos (stages 11–15,  $N=47$ ) had acute VNC axonal defects. Moreover, 55% of the GFP + (mix of heterozygous and WT) embryonic population was also defective ( $N=86$ ), pointing to the dominant negative nature of the  $Rho1^{72F}$  mutant allele. One of those defective GFP + embryos from the balanced germline population of the  $Rho1^{72F}$  line is shown in Fig. 5C as a reference. However, it should be noted that the effects of the heterozygous Rho mutation cannot be unambiguously quantified (Fig. 5C, denoted by “?”) for the above mentioned reason. For the  $Eip63E^{81}$  line, following Mendelian ratios, 2/3 of the embryos would be expected to be heterozygous but since we never observed any defects in GFP+ embryo (mix of heterozygous and WT), we concluded that  $Eip63E^{81}$  heterozygosity does not lead to axon

defects (Fig. 1A, bottom left table, and B bottom right table; Fig. 5B).

We then crossed both the  $Eip63E^{81}$  and the  $Rho1^{72F}$  lines to create embryos heterozygous for both transgenes (GFP –). 22.72% of those embryos showed VNC defects that were of intermediate severity (Fig. 5D). These results suggest that there is indeed functional genomic interaction between the mutant alleles, suggesting that  $Eip63E$  and  $Rho1$  are part of the same metabolic pathway in *Dmel* axogenesis.

We wanted to explore next if the same would happen for simultaneous  $Eip63E$  downregulation and  $Rho1$  overactivation in neurons. Since these experiments would require using the UAS:Gal4 system, no possibility of genotyping embryos using GFP expression was possible, just like for the tissue/time-specific expression experiments. We already observed that neuronal  $Eip63E$  knockdown ( $elavGal4:UASRNAiL63$ ) leads to 49.4% of the embryonic population being defective (50% expected to be expressing the allele) (Figs. 4C, H and 5F) and that it would not

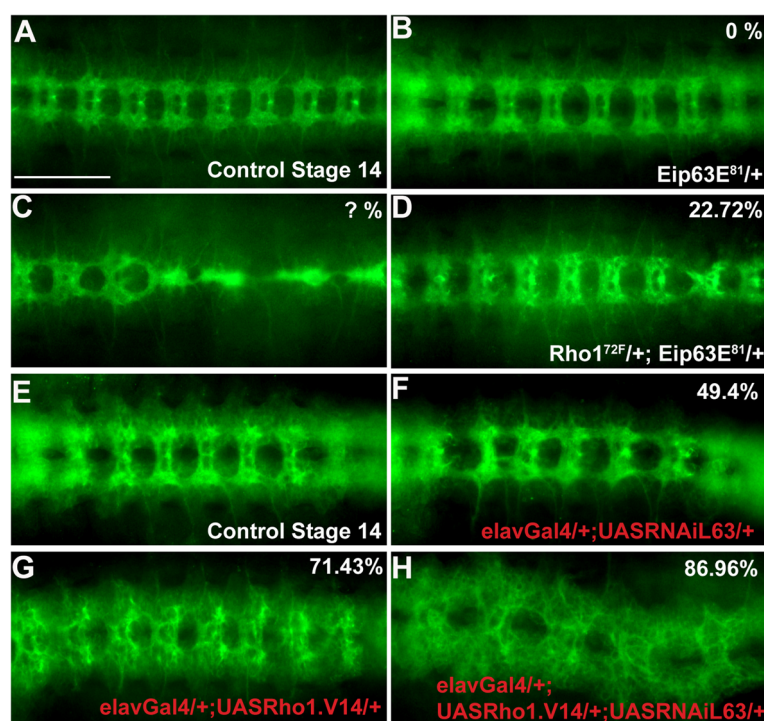


**Fig. 5**  $Eip63E$  functionally interacts with  $Rho1$  to regulate axogenesis. Ventral views of stage 14 whole-mount embryos stained for BP102 antigen are shown head to the left. Panels show representative images for each specified genotype, **A–C** representative images of **A** control embryos, **B** single heterozygous  $Eip63E^{81}$ , and **C** embryo from  $Rho1^{72F}$  line showing defective VNC phenotype (**D**) GFP – embryo from a cross between  $Eip63E^{81}$ -deficient line and dominant-negative  $Rho1$  ( $Rho1^{72F}$ ). **B, C** Images of presumed genotype (see text for details). **D** Axon defects of intermediate severity in 22.7% of embryos heterozygous for  $Rho1^{72F}$  and  $Eip63E^{81}$  (GFP –). **E–H** UAS- $elavGal4$  approach to drive  $Eip63E$  downregulation and constitutive active  $Rho1$  overexpression in neurons in two independent *Dmel* lines. Lines were then crossed to generate the indicated genotypes. Representative images showing VNC defects from  $Eip63E$  downregulated (**F**) or  $Rho1.V14$  expressing (**G**) embryos are presented. 86.96% of all embryos from a cross to generate both  $Rho1.V14$  expression and  $Eip63E^{81}$  knockdown (**H**) show VNC defects. **F, G, and H** are representative images of presumed genotypes (marked in red, see text for details). Penetrance values from stages 13–17,  $n$  as follows: **B** > 100, **C** 86, **D** 22, **F** 89, **G** 126, **H** 69.  $n$  represents the total of screened embryos from several different pairings/collection pools. Scale bar 50  $\mu$ m

lead to any detectable lethality (76 vs 72 adult flies corresponding to absence and presence of balancer phenotypic marker). For Rho1 activation, we used a line expressing a constitutively active Rho1.V14 allele under a UAS promoter. When driven in neurons, 71.43% of the embryonic population showed VNC defects (50% expected to express the allele) and no adult fly ever eclosed that did not show the balancer phenotypic marker ( $N=172$ ) implying a 100% lethality.

We then created a line expressing Rho1.V14 and knocking down Eip63E under UAS promoters and crossed it with a Gal4:elav line to drive neuronal expression. This resulted in 100% lethality since no adult fly ever eclosed that did not show the balancer phenotypic marker ( $n=117$ ). Assessment of the embryonic population following BP102 staining revealed embryonic VNC axon defects in 89.96% of the population with axon phenotypes that resembled a combination of both the controls (Fig. 5H). We detected less axons like those observed in Rho1.V14 control (Fig. 5G) with acute defasciculation and misguidance, just like the RNAiL63 control (Fig. 5F). Since all the individual control phenotypes were present, we conclude that there is a lack of functional interaction between Eip63E deficiency and constitutively active Rho1.

We also examined any functional interaction between Eip63E and the other major members of the Rho family of GTPases, Rac1 and Cdc42 (Additional file 1: Fig. S2). Results show that simultaneous Eip63E neuronal downregulation and activation of Rac1 and Cdc42 (constitutive active forms), but not downregulation (dominant negative forms), lead to the rescue of the control phenotypes. This data suggests that in flies, the Rho family GTPases might be players in the same pathway as Eip63E regulating axonal development. Furthermore, based on our Rho1.V14 data, since Rho1 activation did not rescue the defects associated with heterozygous UASRNAiL63 embryos, our results also point to a role for Eip63E upstream of Rho GTPases, by regulating their activity or that of their regulators.

#### **PFTK1 downregulation and deficiency lead to faster-growing axons in murine cortical neurons**

Previous research using murine experimental models has indicated that CDK5 inactivation leads to inhibition of axonal growth [36, 40] and that CDK-related protein kinase PCTAIRE1-3 negatively regulates neurite outgrowth [41]. We investigated whether manipulation of PFTK1 activity had an impact on axon outgrowth in mammalian cells. Primary cortical cultures from CD1 mouse embryos were infected with adenovirus expressing GFP tagged-D228N PFTK1, GFP tagged-wild type PFTK1, or GFP control alone (Fig. 6A, B). Both at 12 h

and at 24 h after plating, a significant increase in axonal length was observed in cells expressing D228N but not the GFP control or WT PFTK1 (Fig. 6A, B). This suggests an increase in neurite length in vitro upon downregulation of PFTK1 function, contrary to that observed with the loss of CDK5 [40].

We then generated a PFTK1-deficient mouse line to further examine the role of CDK14 in CNS development and maintenance. Details of the generation of the PFTK1 KO mouse line are presented in Fig. S3 and described in the “Methods” section. Unlike PFTK1 deficiency in *Drosophila*, which leads to embryonic lethality, PFTK1 knockout (KO) mice are viable, develop normally, and do not show any obvious morphological defects compared to the wild-type littermates. Microscopic analysis of coronal sections of the adult mouse brain on a mixed C57Bl6 background (3rd generation) revealed no major abnormalities upon cresyl violet staining (Fig. S4A). Furthermore, no noticeable deviation from the expected Mendelian ratios (Fig. S4B) was observed in embryonic or postnatal populations, suggesting that PFTK1 loss alone, in mice, might not have the same effects observed with L63E deficiency in the fly regarding lethality.

Next, to investigate whether the axonal outgrowth effects of D228N overexpression could be replicated by PFTK1 deficiency, we studied populations of axons in primary cortical cultures from PFTK1 KO and WT littermate embryos (Fig. 6C–E). Cultures were prepared from E13.5–14.5 mouse embryos, fixed at 16 and 24 h after plating, and stained for the microtubule marker Tau-1 and Hoechst. The axon length distribution at 16 h in vitro ( $n=13–14$  embryos/genotype, 236–469 cells/embryo) revealed a statistically significant increase in the number of axons longer than 40  $\mu\text{m}$  in PFTK1 KO neurons and a decrease in shorter axons when compared to WT controls (Fig. 6C, D). Nevertheless, the significant difference between KO and WT cultures at 16 h is no longer detected after 24 h in vitro (Fig. 6E), which would suggest that either the effect is transient (early axogenesis) or that axons had reached their maximum possible length in this model at the 24-h mark. Together, these results point to a role of PFTK1 in regulating axon outgrowth during early axogenesis.

#### **PFTK1-regulated axon outgrowth is dependent on RhoA activity**

Based on the functional interaction of Eip63E and Rho GTPases, next, we investigated whether manipulation of RhoA activity in PFTK1 KO neurons could rescue the effects on axonal outgrowth. Under the same settings as the experiments described above (same embryos), PFTK1 KO or WT neurons were treated with RhoA activator CN03, which blocks intrinsic, and GAP-stimulated

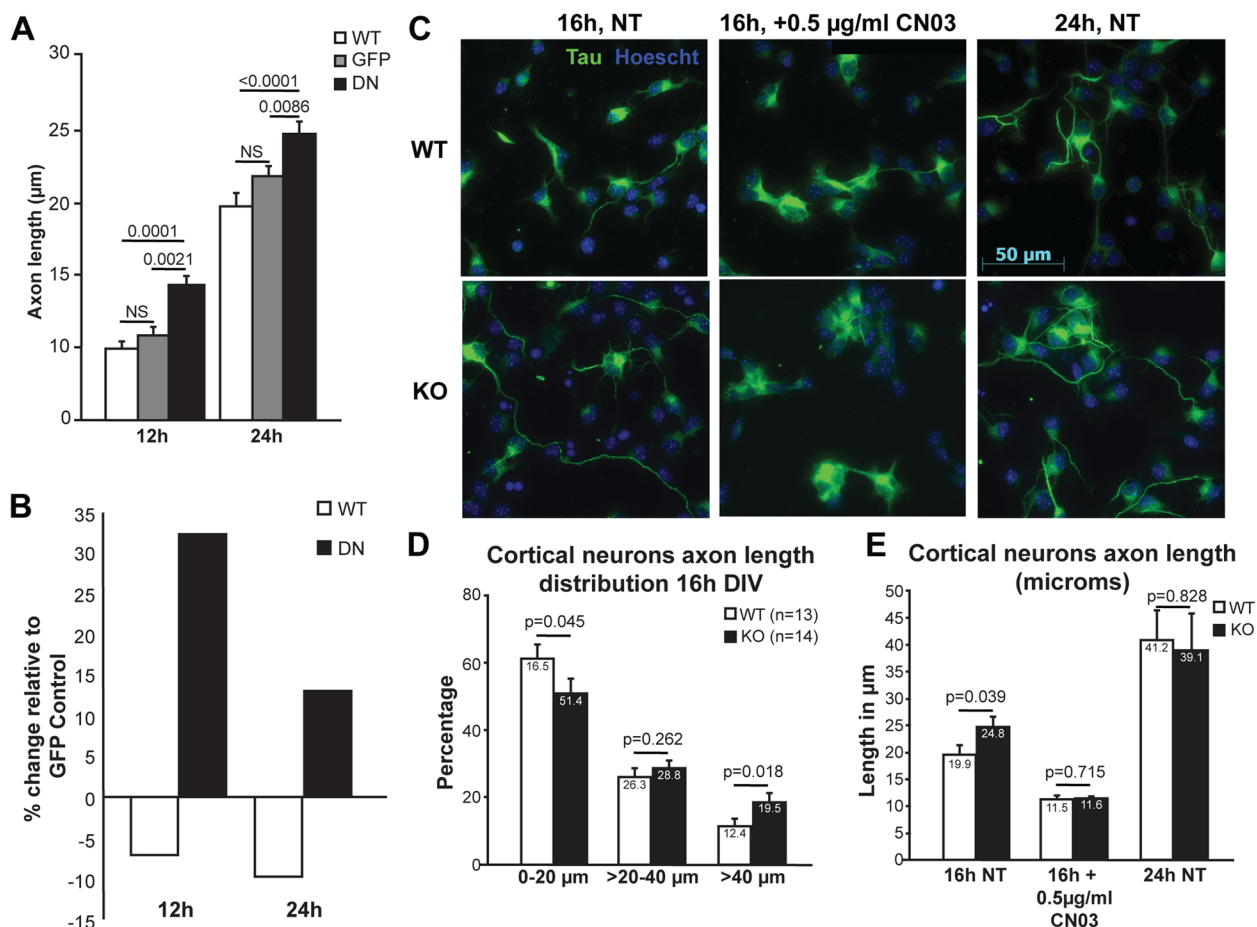


**Fig. 6** PFTK1 downregulation leads to faster-growing axons in murine cortical neurons. Primary cortical neurons derived from CD1 embryos (E 14–15) were infected with 100 MOI of adenoviruses expressing GFP alone, GFP and WT-PFTK1 or GFP and D228N-PFTK1. After 12 or 24 h in culture, cells were fixed and stained with Hoechst 33258 (nuclei visualization). Axons of GFP + neurons were measured using Image J. **A** Values are presented as averages ± SEM from 122–143 cells/treatment/timepoint. Statistics were done using two-way ANOVA followed by Tuckey’s post-hoc. **B** Same data as in **A** but presented as axon length relative to the GFP control. **C** Representative images of primary cortical neurons from E13–14 embryos from HET × HET crosses from WT and KO cultures fixed at the specified times and stained for Tau and Hoechst. **D** Axon length distribution per genotype from the indicated number of embryos (236–469 cells/embryo) at 16 h in vitro. Each column represents the percentage of cells in the specified range of length for the indicated genotype. Non-treated (NT) cultures were also fixed after 16 and 24 h in vitro. Graph represents the average axon length/genotype/treatment. *t*-test was used for statistical analysis whenever *p* value is specified. **E** 16-h cultures were treated for the last 8 h with 0.5 µg/ml of RhoA activator (Cytoskeleton Inc. CN03). Graph represents the average axon length

GTPase activity leading to constitutive activation of RhoA by robustly increasing the level of GTP-bound RhoA [42]. Figure 6C and E show that treatment of the RhoA activator CN03 eliminates the difference between KO and WT cultures by equally decreasing the axon length of both populations of cells (Fig. 6C and E). Consistent with our Dmel results, these data present a strong case for the role of RhoA activity downstream of PFTK1 and the specific involvement of PFTK1-mediated RhoA regulation in axonal outgrowth.

We then assessed whether PFTK1 levels influence RhoA expression. To be as relevant to the axon length experiments as possible, we decided to do the evaluation

in extracts (total RNA and protein) obtained directly from cultured WT and KO cortical neurons (Fig. 7A–C). Reverse transcription polymerase chain reaction (RT-PCR) analysis showed no significant differences in RhoA mRNA level (Fig. 7A and C) in KO vs WT. Surprisingly, examination of the endogenous levels of RhoA protein revealed significantly higher levels of RhoA in PFTK1 KO cortical neurons compared to those of WT (Fig. 7B and C; Fig. S5). This was unexpected, since the genomic interaction experiments in Dmel and the CN03 experiment in cortical neurons were suggesting that PFTK1 deficiency might be leading to less Rho activity. That was also the expectation, since it is very well known that

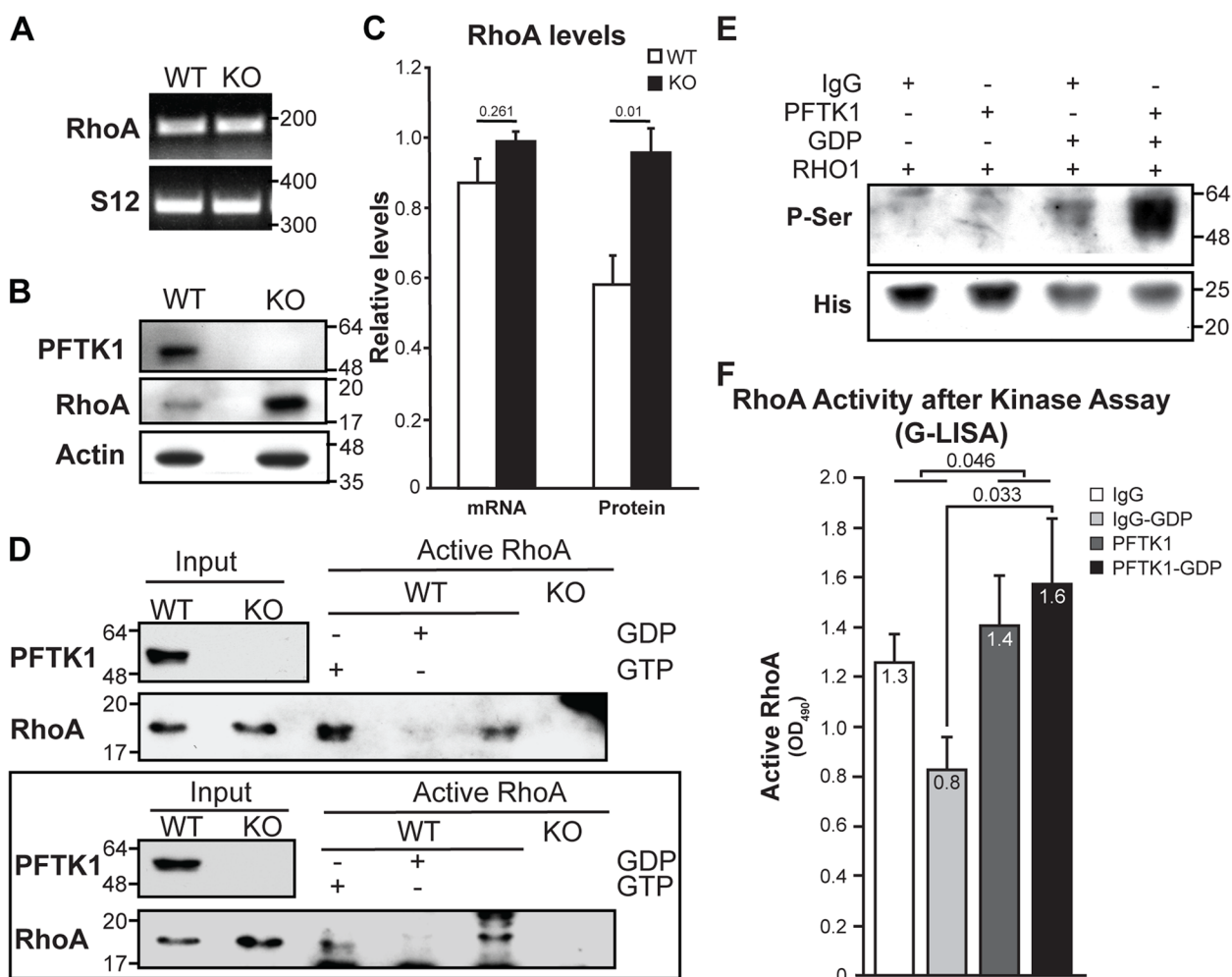


**Fig. 7** RhoA phosphorylation and activity are affected by PFTK1. Neuronal cultures from E13–14 embryos from HET×HET crosses were examined after 18–20 h in vitro. Total RNA (**A**) or protein (**B**) was extracted followed by RT-PCR or western blot. Representative images from RT-PCR (**A**) and western blot (**B**) assays are shown. **C** Bar graph represents the average band intensity from 3 KO and 6 WT for mRNA and 7 WT and KO each for protein. Non-parametric Mann-Whitney test. **D** Assessment of RhoA activity using an IP-based assay. Neuronal extracts were incubated with Rhotekin PBD beads to pull down active RhoA. WT extract preincubated with GTP<sub>γ</sub>S (positive) or GDP (negative) was used as control. IP was followed by western blotting for RhoA. Two representative assays of four independent assays are shown. **E** In vitro kinase assay. IPed protein (either with IgG control or PFTK1) from WT cortical neuronal culture extracts was used as source of kinase and incubated with human recombinant RhoA (His-tagged) with or without GDP. Results were analyzed for phospho-serine signal. **F** RhoA activity assay following in vitro kinase assay. Kinase reactions were analyzed by G-LISA to test for RhoA activity. Bar graph represents mean values ± SEM. Two-way ANOVA analysis of grouped data and Sidak test for multiple comparisons are indicated on bar graph. RHO1, His-RhoA human recombinant protein

lower Rho activity leads to longer axons [43]. Then the question remained of whether the increased levels of RhoA protein in the KO cortex were actually equivalent to increased RhoA activity.

Of note, no significant difference in Rac1 levels was observed between KO and WT cortical neurons (Fig. S5). Nevertheless, preliminary data from performing the same studies using the rest of the brain (no cortex or hippocampus) of the same WT and KO littermate embryos used for cortical cultures suggest that the expression profiles might be inverted. In those extracts, Cdc42 and Rac1

seem to be upregulated in the KO samples vs WT (data not shown).

To answer the pending question, we assessed RhoA endogenous GTPase activity in PFTK1 KO vs WT cortical neurons (Fig. 7D). Briefly, cell extracts were prepared from cortical cultures of PFTK1 wild-type and KO littermates at E13.5–14.5 and then incubated with Rho-binding domain (RBD) of Rhotekin RBD beads, which pulls down the endogenous active form of RhoA from the cell lysate. Active RhoA levels were examined by Western blotting with RhoA antibody. The detected signal

would correlate with RhoA activity and so we expected that the KO signal would be higher than the WT one. Interestingly, despite RhoA protein upregulation in PFTK1 KO mice, we did not detect any RhoA activity in the KO extracts with this technique (Fig. 7D). This suggested that the increased RhoA protein levels in the KO cortex is likely to compensate for the lack or dramatically decreased RhoA activity.

#### RhoA phosphorylation and activity are affected by PFTK1

So far, all our results pointed to a close functional interaction between Eip63E/PFTK1 and Rho1/RhoA but without clarifying if such an interaction was direct. To address this, we decided to test if RhoA is a substrate for PFTK1 (Fig. 7E). Since no recombinant PFTK1 exists yet and it is not clear which and how many cyclins/co-activators it requires to be activated, we were left with the alternative of using cortical neurons extracts from E13-14 WT embryos as source of PFTK1 kinase. Immunoprecipitation would render PFTK1, presumably attached to all relevant co-factors. Optimization of the process was performed using different antibodies, pre-clearing, and incubation times to obtain the cleanest and most PFTK1-enriched sample possible (data not shown). As control, IgG immunoprecipitated samples were used.

Using recombinant His-tagged RhoA as substrate, we then proceeded to optimize an in vitro Kinase assay in the presence or absence of immunoprecipitated PFTK1, followed by Western blot analysis for the resulting reactions using a phosphoserine antibody (Fig. 7E). Noticing the inconsistency of preliminary results that only used the recombinant, we then tested if adding GDP to the reaction mix would stabilize RhoA as a substrate.

Figure 7E shows one representative experiment. In all replicas of the experiment, a noticeable increase in serine phosphorylation of recombinant RhoA was observed only in the presence of PFTK1 and when GDP was externally added to the reaction (Fig. 7E, last lane to the right). These results suggest that recombinant GDP-RhoA is a direct in vitro substrate of PFTK1.

It was important then to determine whether PFTK1 phosphorylation of GDP-bound RhoA had any effect on RhoA activity, since previous reports have shown that depending on the phosphorylation site, RhoA can be activated or deactivated [44–46]. To this effect, we submitted all reaction products of the in vitro Kinase Assay described in the previous experiment (Fig. 7E) to a G-LISA reaction to test for RhoA activity (instead of using them for Western blot). This method, being semi-quantitative and more sensitive than the IP approach used before (Fig. 7D), revealed a significant increase in RhoA activity as a function of PFTK1 compared to IgG control. Additionally, a significant increase in RhoA

activity was observed when GDP-bound RhoA was incubated with PFTK1. These results suggest that GDP-RhoA is not only a substrate of PFTK1 but also that this phosphorylation results in RhoA activation (Fig. 7F). Taken together, these results point to a yet unidentified role of PFTK1 in regulating RhoA activity by phosphorylating and thereby activating GDP bound RhoA.

#### Discussion

The proper development of the CNS requires tight coordination of several important processes including axon development. This is a complex process involving a broad range of factors that are present in the neuronal micro-environment. However, the precise role of PFTK1 in neurite morphogenesis and implications in CNS development has not been fully characterized. Here we present evidence that PFTK1 (Eip63E in *Drosophila*) is involved in this process and mediates its action on axon development by regulating its downstream effector via its kinase activity.

Screening of Eip63E-deficient embryos from two different and independent mutant alleles consistently shows defects in VNC structures. Results (Fig. 1A, bottom panel) showing that the phenotype of the trans-heterozygous embryos is less severe than that of the Df(3L)E1, which contains a larger deletion with at least 2 other background mutations, does indeed suggest that these background mutations have a role in the homozygous Df(3L)E1 phenotypes. Nevertheless, since the only homozygously deleted gene in the trans-heterozygous embryos is Eip63E, our results support the interpretation that the axonal phenotype is linked to Eip63E. This was further confirmed when only neuronal downregulation of Eip63E led to the same VNC defects than those in the mutant germlines. These axon defects occur along neuronal and, to a lesser extent, along glial cell body disorganization. The penetrance values of neuron-related defects are comparable to those of axonal defects already from stage 10 onward (Additional file 1: Fig. S1). This does not seem to be the case for glial defects. No consistent glial perturbations were noticed between the two Eip63E mutant alleles. Taken together, these observations suggest that the axon defects are related to neuronal, rather than glial-related Eip63E functions.

More than one of the CNS markers used to characterize the VNC phenotype of Eip63E KO embryos point to a potential defect in biological processes that regulate or mediate cell identity specification and/or neuronal differentiation processes (Figs. 2B and 3). These defects could be described in general as an abnormal cell cortex laminar organization along the VNC of mutant embryos, a process that is highly dependent on the timing and pattern of progenitors' birth and divisions [47]. It is possible

that defects in Eip63E mutants are related to temporal control of new neurons and/or their differentiation. Indeed, it has been shown before that the absence of cell cycle progression or cytokinesis in neuroblasts leads to abnormal expression pattern of hunchback (Hb) [48], one of the progenitor temporal transcription factors that regulate first-born cell fates in *Drosophila* [47]. Previous reports show that Eip63E has a role in cell cycle regulation, since its downregulation in embryonic cell cultures by RNAi leads to low mitotic index and therefore larger G2 cells [49]. There is also evidence that Eip63E interacts with cyclinY to phosphorylate the low-density lipoprotein receptor-related 6 (LRP6; “arrow” in *Drosophila*) and mediate Wnt signaling [50]; a pathway broadly recognized as essential for regulating progenitor proliferation, cell lineage decisions, and neuronal differentiation in insects and vertebrates [51, 52].

In addition to this early potential function for Eip63E, our data strongly support a later role for this kinase in neurons to regulate axon development. It is evident that early deregulation of differentiation timing would set a precedent for axon defects, since for example, pioneer neurons and axons are needed for correct pathfinding and fasciculation of more mature axon pathways [53]. A key concern for the interpretation of these results is whether axogenesis dysregulation is the primary cause of the axonal defects and not any of the other described phenotypes observed as a result of Eip63E deficiency. The observation that Eip63E downregulation in elav-driven cells (differentiating neurons [54]) is the only tissue-specific downregulation that resulted in VNC defects (Fig. 4C) presents a strong argument for the role of Eip63E in neuronal function. Consistent with this observation, downregulation of Pftk1 in vitro in murine embryonic cortical neurons also resulted in accelerated axon outgrowth. Interestingly in the mouse model, the other observed phenotypes associated with Eip63E deficiency in the fly model, including lethality, were not observed. This suggests that Eip63E could have key functions in other biological processes outside of the CNS in the fly model that might be taken over by other Cdks in mice.

A hypothesis-driven search for functional interactors of Eip63E activity resulted in the identification of RhoA as a potential target. RhoA belongs to the Rho subfamily of GTPases within the Ras superfamily, which also include Cdc42 and Rac1. The family which now includes 20 total members [55] is involved in diverse cellular functions such as the regulation of cytoskeletal rearrangements, cellular motility, cell polarity, axon guidance, vesicle trafficking, and the cell cycle [56]. Most of the Rho family of proteins function as switches that undergo conformational change between the inactive GTP-bound and the

active GTP-bound state. Guanine nucleotide exchange factors (GEFs) activate these Rho GTPases by regulating the dissociation of GDP and the subsequent uptake of GTP from cytosol whereas GTPase-activating proteins (GAPs) facilitate their inactivation by increasing the rate of hydrolysis of GTP. Inactive Rho GTPases in the cytosol are often bound to guanine nucleotide dissociation inhibitors (GDIs) which prevent the GTPases from interacting with their Rho-GEFs at the plasma membrane [57], providing an additional layer of regulation. The role of RhoA in neuronal morphogenesis has been long implicated and has become clearer over the past several years. Although controversial, with initial overexpression studies suggesting inhibition of RhoA activity promoting neurite outgrowth [43, 58, 59], several others [60–62] demonstrate that RhoA activity positively affects neurite initiation and extension resulting in longer axons. Our results side with the former, pointing to a role for PFTK1 in regulating the activation of RhoA leading to more controlled axogenesis. Both expression of a dominant negative form of RhoA and PFTK1 deficiency, resulting in reduced RhoA activity, leads to uncontrolled initiation of axon outgrowth and hence longer neurites.

When Rho1 activity was overexpressed in specific neuronal populations with Eip63E deficiency, VNC defects in axonal defasciculation and misguidance appeared to be additive as both features of Eip63E deficiency (Fig. 5F) and Rho1 constitutive active overexpression (Fig. 5G) could be observed (Fig. 5H). In contrast, simultaneous expression of the constitutive active forms of Rac1 (Fig. S4D) and Cdc42 (Fig. S4J) and Eip63E downregulation in neurons resulted in an intermediate phenotype, implying that Eip63E may be regulating upstream factors that activate Rac1 and Cdc42 and may need further investigations. Intriguingly, in mice cortical neurons, no change in Rac1 expression levels was observed (Fig. S5). One possible explanation for this observed difference between the flies and mouse could be compensation by PFTK2 and PCTAIREs in mice. In flies, in the absence of these homologs, Eip63E emerges to have a dominant role in CNS development and regulation of the activity of Rho family of GTPases. Nevertheless, based on our results with Rho1 activity in flies, we conclude that PFTK1 functions upstream of Rho1, and PFTK1 deficiency results in axonal defects due to perturbations in Rho1 activity.

CDK5 and PCTAIRE, two close family members of PFTK1, have been implicated in axon outgrowth [36, 40]. In our experiments, a noticeable change in axon lengths at earlier time-points (Fig. 6) might indicate that PFTK1 is more important in regulating the initiation of axon outgrowth rather than being involved in axon outgrowth. Interestingly, the percent of neurons with longer axons is higher at 16 h in comparison to 24 h (Fig. 6D). This

indicates that over time, the rate of axonal outgrowth evens out and the effect is lost, suggesting the participation of other downstream factors that regulate axon elongation. Note that this change in axon lengths is not due to generalized effect on the health of the cell as the expression of the dominant negative PFTK1 had no effect on the survival of neurons (Fig. S6).

The lack of any obvious gross CNS phenotype in PFTK1-deficient mice compared to those observed in flies, although intriguing, could be due, in part, to the presence of other PFTK1-related kinases. Flies merely possess the PFTK1 homolog Eip63E but not PFTK2 and PCTAIRE kinases. In comparison, mammals contain both PFTK1 and 2 that show 68% homology, as well as PCTAIRE 1–3, which are 61% homologous to PFTK1 and are all highly expressed in the mouse brain [3, 41, 63, 64]. The presence of these highly similar genes in the mammalian system could compensate for the lack of PFTK1 and result in a lower level of abnormalities in the KO mice. However, the full extent of the effect of PFTK1 deficiency on brain morphology would require a closer examination of specific brain structures. Although the lack of gross developmental defects is not inconsistent with effects on axon length, future analysis of the PFTK1 mice would require a more careful examination.

We observe a noticeable increase in RhoA protein level in PFTK1 KO cortical neurons (Fig. 7B and C) despite no detectable increase in mRNA levels suggesting a posttranslational regulation of RhoA levels. It could be speculated that PFTK1 also plays a role in regulating cellular RhoA levels by regulating RhoA phosphorylation and ubiquitination. In this regard, previous reports have identified specific E3 ligases, Cullin-3, that target GDP-bound RhoA for degradation [65] and further studies may provide clues to the role of PFTK1 in this pathway. Intriguingly, this increase in RhoA level did not translate to more active RhoA but rather a noticeable decrease in detectable active RhoA in PFTK1 KO neurons (Fig. 7D) suggesting that PFTK1-deficient neurons had reduced GTP-bound active RhoA. Additionally, PFTK1 deficiency also resulted in perturbation in axon length of cultured cortical neurons. These results are in line with previous studies that show that reduced RhoA activity leads to longer axons [66]. Combined with the observations that pharmacological activation of RhoA resulted in the loss of the observed difference between PFTK1 WT and KO neurons (Fig. 6E), our data strongly supports a model where PFTK1 regulates RhoA activation which in turn mediates the initiation of axogenesis.

Observations via an *in vitro* kinase assay lend further support to this model (Fig. 7E). Serine phosphorylation of recombinant RhoA by PFTK1 in the presence of GDP

indicates a preference for GDP-bound RhoA by PFTK1. Downstream targets or substrates of PFTK1, other than cyclin Y, that may play prominent role in its function in neurodevelopment, are not currently known. However, our data clearly establishes RhoA as a downstream effector of PFTK1 and identifies regulation of GDP-bound RhoA phosphorylation and activation by PFTK1 as a critical factor in PFTK1-mediated axogenesis. It is intriguing that the addition of GDP to purified recombinant RhoA would have any effect on RhoA activity as purified RhoA is expected to already be in the GDP-bound state due to RhoA's intrinsic GTPases activity. It should be noted that adding GDP to recombinant RhoA in the absence of Pftk1 resulted in reduced RhoA activity (Fig. 7F) suggesting a potential exchange of nucleotide under the conditions employed. Given that the addition of GDP resulted in increased phosphorylation of RhoA, it should be noted that regulation of Cdk family of proteins, of which Pftk1 is also a member, by GDP is not known in published literature.

Accumulating evidence suggests the importance of the regulation of Rho GTPases phosphorylation in its function [44, 67]. In this regard, it will be critical in future studies to address potential phosphorylation sites on RhoA, regulated directly or indirectly by PFTK1. All our attempts to address those questions did not render consistent results, as the approaches (GC-MS, targeted RhoA mutagenesis) were impeded by the complexity of obtaining reliable immunoprecipitated PFTK1 samples. Preliminary data suggest that the PFTK1 targeted site is conformational in nature, but more exhaustive experiments need to be done and a more powerful approach applied to be able to answer this question. Based on our evidence, it is also difficult to rule out the regulation of other upstream factors by PFTK1 that may mediate RhoA activity. This would add a further mode of regulation of RhoA function by PFTK1.

## Conclusions

In this report, we present convincing evidence that PFTK1/Eip63E plays an important role early in neurogenesis. PFTK1 accomplishes this role in mediating axogenesis by phosphorylating and regulating the activation of RhoA, well-known for its diverse cellular function including axon development. Taken together, the evidence presented here proposes a working model for PFTK1 in mediating neuronal polarization and axon growth via RhoA regulation, pointing to the only known activating phosphorylation of RhoA with a role in axogenesis.

## Methods

### *Drosophila* strains

Flies were kept under standard conditions. Stocks are described in FlyBase (<http://flybase.bio.indiana.edu>). The following stocks were obtained from the Bloomington stock center: W1118, Eip6381/TM6tb, Df(3L)E1/TM6, Rho1<sup>72F</sup>, green balancer flies (L2Pin1/CyokrGFP, D\*gl3/TM3krGFP, In(2LR)nocSco,b1/CyoActGFP and Sb/TM3ActGFP,Ser), and Gal4 driver lines (elav::Gal4, Repo::Gal4/TM3,Sb, elav::Gal4;UAS::Dcr2.D and UAS::Dcr2.D;Act5::Gal4/Cyo). Three independent RNAi *Drosophila* lines were obtained from the Vienna *Drosophila* RNAi Center (UAS::RNAiL63/Cyo, UAS::RNAiL63 and UAS::RNAiL63/TM3,Sb). For the purpose of mutant embryo characterization, the TM6 balancer in both Eip63E-deficient lines [9] was replaced with the TM3. Kruppel-GFP balancer chromosome [15]. To perform Eip63E-specific downregulation, the Gal4:UAS system was used [34]. Balancers in all UAS and Gal4 lines involved in the cross strategies were changed for the Actin5c-GFP balancer chromosomes (Cyo or TM3 as needed) [35].

### *Drosophila* immunohistochemistry

*Drosophila* embryos from Eip63E mutant lines were collected for 2 h on grape juice-agar medium [68] and allowed to carry on development to embryonic stages 6–15 [69], in batches including only 2–3 stages each, by further incubation at 25°C. This developmental window includes all events of embryonic CNS development, from anlage formation to differentiation and axogenesis [20]. Whole-mount embryos were prepared following standard procedures [70]. Embryos were dechorionated with 50% bleach, followed by fixation for 20 min in heptane saturated with 4% Paraformaldehyde in 136 mM NaCl, 2.68 mM KCl, 10.14 mM Na<sub>2</sub>HPO<sub>4</sub>, 1.76 mM KH<sub>2</sub>PO<sub>4</sub>, pH 7.4 (PBS). Vitelline membrane was removed by vigorously shaking the fixed embryos in methanol, followed by further methanol washes. Embryos were re-hydrated using PBS-0.1% Triton X-100 (PBT) and then blocked for 20 min using 20% Normal Goat Serum (NGS) (GE Healthcare, Amersham RPN410) in PBT. Fluorescence co-immunostaining was performed against GFP (to amplify the presence of the balancer embryonic marker), HRP, and a CNS marker. Primary antibodies were as follows: mouse anti-GFP (JL-8, Living colors, 1/100), Cy3-anti-HRP (1/25), mouse BP102 (1/10), mouse anti-En/Inv (4D9, 1/10), mouse anti-single-minded (1/5), mouse anti-Futsch (22C10, 1/10), mouse anti-Neuroglian (BP-104, 1/10), mouse anti-elav (9F8A9, 1/14), and mouse anti-Repo (8D12, 1/10). All monoclonal antibodies against CNS markers were obtained from the Developmental

Studies Hybridoma Bank developed under the auspices of the NICHD and maintained by The University of Iowa, Department of Biology, Iowa City, IA 52242. Such antibodies were developed by C. Goodman, S. Crews, S. Benzer, and G.M. Rubin. Since the anti-HRP antibody was Cy3-conjugated, only Alexa 488-Goat anti-mouse (1/100) was used as secondary antibody, after a second blocking step. Stained embryos were then directly mounted in Vectashield (Vector laboratories, H-1000) and visualized under a fluorescent microscope.

Embryo dissections were performed essentially as described [71]. Seven- to 13-h timed embryos were transferred to a piece of double-sided tape mounted on a polylysine-covered microscope slide and then rolled using forceps to mechanically remove the chorions. Embryos were then covered with PBS and examined under fluorescence light for GFP expression. The absence of GFP expression would indicate an Eip63E deficiency. After genotyping and fine determination of developmental stage based on morphological features, a dorsal incision was made in the vitelline membrane of each with a sharpened tungsten needle (Small Parts Inc TW-006–60). Each embryo was then removed from the membrane and placed ventral side down directly on the polylysine-covered surface of the slide, while still submerged in the PBS. Using the tungsten needle, an incision was made longitudinally along the dorsal surface of the embryo and the body walls were pressed down onto the glass. The gut and remaining yolk sac were then removed, resulting in a flat embryonic preparation. Dissected embryos were then fixed for 30 min at room temperature in 4% paraformaldehyde in PBT. One-hour blocking was performed using 10% NGS in PBT, followed by antibody staining. Fluorescence co-immunostaining was performed against HRP and a CNS marker. Same antibodies mentioned above were used but at different concentrations: 1/50 for primary antibodies and 1/300 for secondary. Preparations were mounted using Fluoromount<sup>TM</sup> mounting media (Sigma F4680), sealed with clear nail polish, and visualized under a fluorescent microscope.

### Transgenic mouse systems

All experimental animal studies were conducted in accordance with the guidelines of the University of Ottawa Animal Care Committee and University of Calgary Animal Care Committee and conformed to the guidelines set forth by the Canadian Council on Animal Care and Canadian Institutes of Health Research.

### Generation and analysis of PFTK1 transgenic (knockout) mice

PFTK1 heterozygote mice were generated by the Gene Targeting and Transgenic Facility of Texas A&M Institute

for Genomic Medicine (TIGM), on mixed (129/SvEvBrd x C57BL/6) background. To generate the mutant allele, PFTK1 Gene (MGI: 894,318) and the transcript sequence of PFTK1 or (Cdk14-002 ENSMUST00000030763) located on chromosome5 (4,803,391–5,380,197) (reverse strand) was targeted. The intron–exon structure of the PFTK1 gene obtained by genomic mapping is illustrated in Fig. S3A. PFTK1 heterozygotes were generated by replacing the majority of exon 6 of the *Mus Musculus* PFTK1 transcript (ENSMUST00000030763) starting from nucleotide 18 with the neomycin (Neo) resistance cassette via homologous recombination. The resulting insertion in the PFTK1 gene causes a frame shift altering the open reading frame and leading to a premature stop codon which produces a truncated protein without the entire kinase domain. The correct integration of the targeting sequence within the *Pifraire1* gene was confirmed by Polymerase Chain Reaction (PCR) and Southern blot hybridization analysis in the 129/SvEvBrd embryonic cells that were transformed (Fig. S3B). Following Bgl II or Acc65 I restriction digestion of the genomic DNA, Southern blot was performed using probes targeting 5' or 3' regions outside of the targeting vector, respectively. The predicted band sizes of 15.9 kb after Bgl II digestion with the 5' probe and 13.5 kb after Acc65 I digestion with the 3' probe confirm the homologous recombination of the external cassette. The transformed PFTK1 allele was easily detectable in the transformed mice through the agouti coat color of the chimeras. The produced chimeric mice were viable and fertile; after being crossed with wild-type mice, they also produce the PFTK1 heterozygote-deficient mice that were viable and fertile. PFTK1 F1 generation, homozygote (null) mice, which were obtained by breeding heterozygous parents, were also viable and fertile. To establish PFTK1 knockout line on a pure C57BL6 background, we backcrossed mixed (129/SvEvBrd x C57BL/6) heterozygote mice from the PFTK1-deficient line with C57BL6 for 10 generations, which continue to be viable. PCR performed on tail genomic DNA samples obtained from PFTK1 wildtype, heterozygote, and knockout PFTK1 mice and the corresponding primer pairs (fwd. 5'-TGACCCCTGTCTTTG AATACGTG-3' and rev. 5'-GGAAGCCTAAATTGT AAGGATCAGG-3' generating a 418-bp wild-type fragment and fwd. 5'-GCAGCGCATCGCCTTCTATC-3' and rev. 5'-GGAAGCCTAAATTGTAAGGATCAGG-3' generating a 341-bp fragment) are presented in Fig. S3C.

PCR mix was run with GoTaq Green Master Mix 2x (Promega, M712B). The PCR amplification process was as follows: initial amplification designed as touchdown PCR including 6 cycles of denaturation 98 °C for 17 s, annealing 69 °C (touchdown, –1 °C per cycle) for 15 s, amplification 72 °C for 15 s, and further amplification

of the target genes was as follows: 35 cycles of 98 °C for 17 s, 60 °C for 15 s, and 72 °C for 15 s. PCR products were resolved on a 1.5% agarose gel- Ultra Pure Agarose (Invitrogen, 15,510–027) and visualized by ethidium bromide (Ethyl hexadecyl dimethyl bromide C<sub>20</sub>H<sub>44</sub>BrN) (Sigma Ultra, C5335-1000).

#### Real-time PCR (quantitative RT-PCR)

All steps were performed in RNAase-free environment. To ensure RNA-free surface, RNase away (MBP Molecular Bioproducts, 7003) was applied. Total RNA was extracted from mouse embryo whole brains/cortices at embryonic day E 13.5–14.5 using Trizol Reagent (Ambion, 15,596,026) based on Invitrogen protocols. 25 ng of extracted RNA was used per reaction. To determine the disruption of PFTK1 transcription, the SuperScript III Platinum SYBR Green One-Step RT-PCR kit (Invitrogen, 204,174) was used. Negative controls, no RNA, and no RT were run in parallel with both the GAPDH housekeeping gene and PFTK1. Each sample was run in quadruplets and  $n=3$ . Results were normalized against GAPDH. Primers used for amplification of the target genes were as follows: (GAPDH-Fwd.: 5'-GGT GAAGGTCGGTGTGAACG-3', GAPDH-Rev: 5'-CTC GCTCCTGGAAGATGGTG-3') to generate a 233 bp product and (PFTK1-Fwd: 5'-CAGCGATCTGCCTCC ACGGC-3') designed within exon13. (PFTK1-Rev: 5'-GGCCCTCATGCTCTCTCCAGC-3') designed within exon 14, to generate a 341-bp product. The primers would also be able to produce a short heptamer within mutated region (exon 8); thus, it could not interfere with mRNA levels for PFTK1-KO. The program for RT-PCR amplification was as follows: 48 °C for 30 min, 95 °C for 10 min, and 40 cycles of 95 °C for 15 s, 60 °C for 30 s, and 72 °C for 30 s. The RT-PCR products were resolved on a 1.5% agarose-ethidium bromide gel as well.

#### Cell culture

Human Embryonic Kidney cells (HEK-293 T) were cultured in Dulbecco's modified Eagle medium (DMEM) (high glucose 4500 mg/L with 4 mM L-glutamine without sodium pyruvate 0.1 µm sterile filtered) (ThermoScientific, SH30022-01) supplemented with 10% fetal bovine serum (FBS) (Hyclone, SH30397.03) and 1% antibiotic/antimycotic solution 100×(10,000 units/ml of penicillin, 10,000 µg/ml of streptomycin, and 25 µg/ml of Amphotericin B, 0.2 µm filtered) (ThermoScientific, SV30079.01) at 37 °C in a 5% CO<sub>2</sub> atmosphere.

#### Primary cortical neuron cultures

Cortical neuron cultures were prepared either from wild-type CD1 mouse embryos purchased from Charles River or from heterozygous crosses between PFTK1 mice, at

gestational day /embryonic day E 13.5–14.5. Embryos were considered E 0.5 d, at the time the vaginal plug was detected. Embryos were removed from the uterine horns and transferred to Hanks' Balanced Salt Solution (HBSS) (modified without Calcium and Magnesium) (Hyclone Gibco, SH3003102). Brains were excised by cutting the skull open at the midline, from the base of the head towards the front. Two lateral incisions were made under the cerebral cortices, the skull was peeled off, meninges were removed, and individual cortices were transferred to HBSS containing 8  $\mu$ l Trypsin (25 g/L in 0.9% NaCl) (Sigma, T4549), incubated for 20 min at 37 °C with agitation. 10.7  $\mu$ l of Trypsin inhibitor in Neurobasal medium was added to stop trypsinization, and 13.34  $\mu$ l DNase1 (10 mg/ml) (Boehringer Mannheim Roche Diagnostics, 10,137,100) to degrade extracellular DNA medium were added to the solution. Cells were pelleted at 1000 $\times$ , for 5 min at 4 °C, and 10.7  $\mu$ l of trypsin inhibitor and 13.34  $\mu$ l of DNase were added. Cells were triturated; viable cells were counted using sterile filtered trypan blue solution (0.4%) (Sigma, T8154). (Number of cells per ml was calculated by: cell count in the central square $\times$ dilution factor $\times$ 104.) Cells were diluted to the desired concentration for culture, in Complete Neurobasal Medium containing: Neurobasal medium (Gibco LifeTechnologies, 21,103–049), B27 supplement (Invitrogen, 17,504–044), N2 supplement (Invitrogen, 17,502–048), L-Glutamine 200 mM (Gibco, 25,030–081), and penicillin–streptomycin. Primary cortical neuron cells were plated into 24- or 6-well plates. Plates were coated with poly-D-lysine-hydrobromide (1 mg/ml, sterile) (Sigma, P0899) prior to use. Poly-D-lysine incubation was performed for at least 30 min and then plates were washed. For immunostaining, sterilized coverslips were placed into 24-well culture dishes and then coated with poly-D-lysine. Cultures were incubated at 37 °C in a 5% CO<sub>2</sub> atmosphere and fixed or lysed at varied times.

### Expression vectors

Plasmids for transfection: GFP subcloned into pCig2 vector (generously gifted by Carola Sherman); FLAG-Tagged: WT- PFTK1 and D228N- PFTK1 cDNA (mutation of conserved aspartic acid residue to asparagine, by a point mutation) (1284 kb) subcloned into pCMV vector (generously gifted by Dr. Paul Albert and Maribeth Lazzaro) [72]; GST-Tagged: WT-Rac1, G12V-Rac1, S17N-Rac1 subcloned in pEBG vector; GST-tagged: WT-Cdc42, G12V-Cdc42, S17N-Cdc42 subcloned in pEBG vector; and MYC-tagged: WT-RhoA, CA-RhoA Q63L, DN-RhoA L19N in pRK5 vector. Rho GTPases (generously gifted by Dr. Gary Bokoch and Dr. Margaret Chou, University of Pennsylvania). Constructs were sequenced at Ottawa Genomic Center, using following primers: (1)

for Rac1 and Cdc42 constructs in the pEBG backbone: (pGEX 5' sequencing primer: 5'-[GGGCTGGCAAGC CACGTTTGGTG]-3' and pGEX 3' sequencing primer 5'-[CCGGGAGCTGCATGTGTCAGAGG]-3'), and (2) to sequence PFTK1, CMV virus backbone: (pCMV 5' sequencing primer: 5'-CGCAAATGGGCGGTAGGC GTG-3' PFTK1 GC rich region at 3' end: 5'-GGGGGA GTTGAAGCTGGCAG-3'). Sequencing was performed 100 bp upstream of start codon and 100 bp downstream of stop codon. Plasmids were transformed with Top10 competent cells. Transformed cells were cultured on ampicillin-resistant agar plates (LB Agar Granulated, Molecular Genetics BP-1423–500). A single colony was picked and grown in Luria–Bertani (LB) Broth (Miller Amresco, J-106-500G). DNA was purified using the Pure Yield Plasmid Midi Prep System (Promega, A2495).

### Transient transfection with lipofectamine

HEK 293 T cells were cultured to 70% confluency, then co-transfected with Flag-tagged (WT- PFTK1 or D228N-PFTK1) and GST-tagged [WT-Rac1, G12V-Rac1 (constitutively active), S17N-Rac1 (dominant negative inactive)] or GST-tagged [WT-Cdc42, G12V-Cdc42 (constitutively active), S17N-Cdc-42 (dominant negative inactive)] or GST tagged [WT-RhoA, Q63L- RhoA (constitutively active), L19N-RhoA (dominant negative inactive)], as well as, the reporter vector (GST::PEGB, MYC::PRK5, Flag::CMV using lipofectamine 2000 reagent (1 mg/ml) (Invitrogen, 11,668–019). Opti-MEM (Minimal Essential Medium), 1 $\times$ Reduced Serum (Gibco, 31,985–070) was used to dilute the plasmid and lipofectamine according to the manufacturer's instructions. Diluted plasmid and lipofectamine were mixed and incubated for 20 min at room temperature. Cell culture medium was changed to media without FBS at the time of transfection. The plasmid-lipofectamine complex was added to culture media in droplets. Twenty-four hours post-transfection, cells were triturated off culture plates by scraping, and cells were collected into ice cold PBS and spun down at 1.4 $\times$ g for 1 min for pull-down assay.

### Viral infection

Gene delivery via adenoviral (AV) infection was performed at the time of plating. Adenovirus expressing WT-PFTK1 (Ad ET-CMV-3 $\times$ Flag-WT- PFTK1, Pfu: 1.00 $\times$ 10<sup>12</sup> CsCl Pure, Plaque pure), D228- PFTK1 (Ad ET-CMV-3 $\times$ Flag-D228N-PFTK1, Pfu: 9.20 $\times$ 10<sup>11</sup> CsCl Pure, Plaque pure), and GFP (Ad ET-CMV-EGFP, Pfu: 4.89 $\times$ 10<sup>11</sup> CsCl Pure, 3 $\times$ Plaque pure) was mixed with neuronal cortical culture cells at 50–100 MOI (multiplicity of infection). Cells were fixed or lysed, at different time points, post-culture, for further analysis, depending on the nature of the experiment.

### Neuronal death assay

Cortical culture cells from mouse embryos at E13.5–14.5 were seeded at ( $1 \times 10^5$ ) in 96-well plates and infected/co-infected with AV viruses (GFP alone or GFP+WT-PFTK1, D228N-PFTK1) at MOI=100 at the time of plating, for survival assay. Cells were washed with 1X PBS and then fixed with 4% PFA 12, 16, and 24 h post-infection and then stained with Hoechst 33,258 (1:10,000) (Sigma-Aldrich B2883) in 1X PBS and incubated for the minimum of 30 min for nuclei staining. Intact nuclei were counted against condensed and fragmented nuclei to determine live neurons versus dead ones. To determine survival, the number of live GFP-positive neurons were assessed in each well, each treatment was performed in triplets, and the average for each treatment was calculated. Survival was assessed for WT-PFTK1 or D228N-PFTK1 as the percent of live GFP-positive neurons in comparison to GFP. Survival percentage represents the ratio of GFP-expressing neurons with morphologically intact nuclei at 12, 16, and 24 h in WT-PFTK1 or KO-PFTK1 to the total number of GFP-expressing neurons. The values were normalized to GFP alone as control. Data are presented as mean  $\pm$  SEM of at least three independent experiments.

### Total protein extraction

To compare protein expression levels, whole brain lysates were prepared from mouse brains at E13.5–14.5 or from mouse pups at P21. Basically, mouse brains were dissected and washed with ice-cold PBS. Brains were homogenized in lysis buffer: [50 mM Tris-HCl (pH=7.5), 150 mM NaCl, 1 mM MgCl<sub>2</sub>, 1 mM EDTA, 1% Triton X-100 (Boehringer Mannheim, 789,704), 1 mM L-Dithiothreitol (DTT, C4H10O2S2) (Sigma-Aldrich, D0632-5G), protease inhibitor (Halt Protease inhibitor Cocktail EDTA-free 100x (Roche, 87,785))] for 20 min, at 4 °C, with agitation. Lysates were clarified by centrifugation at 19,500  $\times$ g, 4 °C, for 20 min. Supernatant was collected (approximately 2 mg of protein was collected per brain), mixed with 0.1% w/v bromophenol blue/ DTT sample buffer, and heated at 100 °C, for 10 min.

### Immunoprecipitation (IP)

All steps were performed on ice. Cell lysate was prepared as described, previously. Lysate was prepared using lysis buffer 50 mM Tris-HCl (pH=7.5), 150 mM NaCl, 1 mM MgCl<sub>2</sub>, 1 mM EDTA, 1% Triton X-100 (Boehringer Mannheim, 789,704), 1 mM DTT (L-Dithiothreitol, C4H10O2S2) (Sigma-Aldrich, D0632-5G), protease inhibitor, for 20 min, at 4 °C with agitation. Lysates were clarified by centrifugation at 19,500  $\times$ g, 4 °C, for 20 min. Supernatant was collected and incubated with 20  $\mu$ l of washed bead per reaction. After immunoprecipitation,

beads were pelleted at 1000  $\times$ g, washed five times with wash buffer (Tris-HCl (pH $\approx$ 7.3–7.5), NaCl, EDTA, Triton 10%, DTT), then mixed with 0.1% w/v bromophenol blue/DTT sample buffer, and heated at 100 °C, for 10 min to release the protein complex. Proteins were resolved on 12% SDS-polyacrylamide gels.

For immunoprecipitation of ectopically expressed GST tagged proteins, GST beads (Glutathione Sepharose 4b beads, particle size 45–165  $\mu$ m, GE Healthcare 17-0756-05) were incubated with the lysate overnight, at 4 °C, on a rotor. For immunoprecipitation of endogenous protein, Trueblot Anti Rabbit IgIP beads (eBioScience, 00-8800-25) or Anti mouse IgIP beads (eBioScience, 00-8811-25) were used, depending on the origin of the bait antibody. Lysate was collected and precleared by incubating 20  $\mu$ l of the washed bead that was to be used for IP, for 30 min, at 4 °C, on a rotor. Supernatant was cleared by centrifugation at 1000  $\times$ g, 1 min, at 4 °C. 4–8  $\mu$ g of antibody per reaction, normal mouse IgG (SantaCruz, sc-2025) or normal rabbit IgG (SantaCruz, sc-2027) and Pftaire-1 (H-140) (1:500) rabbit polyclonal IgG (SantaCruz, sc-50475), RhoA (1:500) mouse monoclonal IgG (SantaCruz, sc-418), Rac1 (C-11) (1:500) rabbit polyclonal IgG (SantaCruz, sc-95), and Cdc42 (1:500) rabbit polyclonal IgG (SantaCruz, sc-87) were incubated with the cleared supernatant, overnight, at 4 °C, on a rotor. PFTK1 was used to IP GTPase and vice versa. 20  $\mu$ l of the washed beads was incubated with the antibody-lysate mix for 3 h, at 4 °C, on a rotor to precipitate the antibody.

### SDS-PAGE and Western blot

Protein extracts were resolved on a 10 or 12% SDS-polyacrylamide gel, along with Molecular Marker, Blueye Prestained Protein Ladder (GeneDirex, P14007-0500). Transfers were done on 0.45  $\mu$ m PolyVinylidene DiFluoride (PVDF) Transfer membrane (Immobilon-P, IPVH00010). Membrane was blocked in 10% non-fat dry milk in 1X PBST [phosphate buffered saline (pH=8.0) and 0.1% Tween] at room temperature, for 1 h. Proteins were detected using antibodies. Primary antibodies were diluted in [3% bovine serum albumin (BSA) fraction V (Fisher, BP1600-100) in PBST and 0.1% Sodium Azide NaN<sub>3</sub> (Sigma Ultra, s-8032)] as follows: PFTK1 (H-140) (1:500) rabbit polyclonal IgG (SantaCruz, sc-50475), Pftaire2 (CDK15) (1:500) rabbit polyclonal (Life Span Biosciences, LS-C119219/34326), RhoA (1:500) mouse monoclonal IgG (SantaCruz, sc-418), Rac1 (C-11) (1:500) rabbit polyclonal IgG (SantaCruz, sc-95), Cdc42 (1:500) rabbit polyclonal IgG (SantaCruz, sc-87), Cdk5 (C-8) (1:500) rabbit polyclonal IgG (SantaCruz, sc-173), Pctaire1 (CDK16) (1:500) rabbit polyclonal (Life Span Biosciences, LS-C112292/34325), Anti-Flag (1:500) rabbit monoclonal IgG (Sigma, F7425), Anti-GST (1:500)

mouse monoclonal IgG (SantaCruz, sc-138), and incubated with the membranes overnight, at 4 °C, with agitation. Membranes were washed and then incubated with secondary antibodies diluted in 5% non-fat milk, for 1 h, at room temperature [goat anti-mouse 170–6516 or goat anti-rabbit 170–6515 IgG (H+L) HRP conjugate (Bio-Rad)] were all used at 1:2000 in 3% BSA in 0.1% Tween 20 (PBS/T). Immunoreactivity was detected using Immobilin Western Chemiluminescence HRP substrate (Millipore, WBKLS0500) or Pierce ECL Western Blotting Substrate (Thermo Scientific, 32,106) and visualization HyBlot CL Autoradiography film, Denville Scientific. Protein levels were normalized against  $\beta$ -actin signals, and results were reported in reference to control values (untreated control for each individual experiment).

#### **PFTK1 kinase assay**

Kinase assay was performed using immunoprecipitated WT-PFTK1 protein or IgG as a control. Briefly, neuronal cortical cells prepared from WT-PFTK1 mouse embryos E13.5–14.5 were cultured in Neurobasal media (Gibco, 21,103–049) containing B27 (Invitrogen, 17,504–044) and N2 (Invitrogen, 17,502–048), in 12-well plates, at the ratio of 1 embryo per well, for 18–20 h, at 37 °C, 5% CO<sub>2</sub>. After washing with ice-cold 1×PBS, lysates were collected directly from plates by scraping into ice-cold immunoprecipitation (IP) buffer (Tris–HCL 25 mM (pH 7.4), Na<sub>4</sub>P<sub>2</sub>O<sub>7</sub> 10 mM, Na<sub>3</sub>VO<sub>4</sub> 25 mM, NaF 50 mM, EDTA 1 mM, Digitonin 2 mg/ml) and sonicated twice, for 3 cycles, with a 20-min incubation in between the 2 set of cycles, and then supernatant was cleared by centrifugation at 14,000×g, 4 °C, for 10 min. 1 mg of protein (adjusted to the volume of 300  $\mu$ l) was incubated with 4  $\mu$ g antibody either normal rabbit IgG (200  $\mu$ g/0.5 ml) or PFTK1 (200  $\mu$ g/ml) antibodies, overnight, at 4 °C, on the shaker. IP-ed, WT-PFTK1, and IgG were mixed with 40  $\mu$ l of pre-equilibrated (performed washes with IP wash buffer) Trueblot anti-rabbit IgIP beads per reaction and incubated for 2 h, at 4 °C, on the shaker. Beads were then washed and pelleted at 2000 rpm, for 1 min, at 4 °C, with IP wash buffer and kinase assay buffer [HEPES 50 mM (pH 7.5) and 1 mM DTT], respectively. Next, kinase reaction buffer (HEPES 50 mM (pH 7.5), 1 mM DTT, 10 mM MgCl, and 20  $\mu$ M ATP) was added to a final volume of 25  $\mu$ l. 10  $\mu$ g of RhoA substrate His-Recombinant human RhoA (Prospec, pro-057) was added to reactions with or without (5  $\mu$ l, 100 x) GDP. Reactions were incubated overnight, at 30 °C. Samples were then centrifuged at 2000 rpm, for 1 min, at 4 °C, then supernatant was collected and subjected to either Western blot for rabbit polyclonal IgG phosphoserine (Invitrogen, 61–8100) signal or G-LISA assay to assess RhoA activity as described below.

#### **Assessment of Rho GTPase activity**

Activation of RhoA, as a function of PFTK1 kinase activity, was determined using commercially available “RhoA Activation Assay Kit (CellBioLabs, STA-403-A)” according to the manufacturer’s instructions. Primary Cortical Culture Cells were prepared from Het×Het crosses at embryonic day 13.5–14.5, at the density of 1 embryo per well, in 1.5 ml, cultured in complete Neurobasal media supplemented with B27 and N2, in 12-well plates, and incubated at 37 °C and 5% CO<sub>2</sub>. Eighteen to 20 h post-plating, cells were washed with ice-cold PBS and GTPase assay was performed according to the manufacturer’s kit. To decrease rapid hydrolysis of active GTP-bound to inactive GDP-bound protein, all the following procedures were performed on ice. Briefly, cells were incubated on ice, for 20 min, with 1×Assay/lysis buffer provided with the kit (Part No. 240102) (containing 125 mM HEPES, pH 7.5, 750 mM NaCl, 5% NP-40, 50 mM MgCl<sub>2</sub>, 5 mM EDTA, 10% Glycerol) and then collected by scraping. Due to the very low expression of RhoA, same-genotype extracts were pooled to achieve large amounts of Protein. Total protein was quantified by Bradford protein assay to achieve at least 800ug of protein for each sample/assay. Cell lysates were clarified by centrifugation at 14,000×g, at 4 °C, for 10 min (at least 800  $\mu$ g protein per reaction). 100×GTP $\gamma$ S (Part No. 240103) and GDP (Part No. 240104) were added to the cells for positive and negative control, respectively. Control samples were incubated for 30 min, at 30 °C, with agitation, and the reaction was terminated by adding 1 M MgCl<sub>2</sub> to the samples. Volume of sample per reaction was adjusted to be identical in all reactions and 40  $\mu$ l of bead was added per reaction. Active proteins were immunoprecipitated with respective rhotekin RBD agarose beads for RhoA. Beads were pelleted by centrifugation at 14,000×g, for 10 s, and washed three times with 1×Assay buffer supplied in the kit. Afterwards, beads were resuspended in SDS-PAGE sample buffer and boiled for 5 min for detection by Western blotting. Separated proteins were visualized using RhoA, Mouse Monoclonal antibody (Part No. 240302) provided with the kit.

To quantify Rho GTPase activity after the PFTK1 Kinase assay, in a more accurate/sensitive manner, G-LISA RhoA activation assay biochem kit (Absorbance based) (Cytoskeleton, BK124) was used according to the manufacturer’s protocol. Samples from the kinase reactions (IgG-IP: RhoA, IgG-IP: RhoA+GDP, PFTK1-IP: RhoA and PFTK1-IP: RhoA+GDP) were diluted and pre-equalized with ice-cold lysis buffer /binding buffer (Part #GL37). To pre-equalize samples, protein concentration was determined at 600 nm, using Precision Red™ Advanced Protein Assay Reagent (Part # GL50) as suggested by the manufacturer. Same buffer mix (no

protein) and RhoA (provided by the manufacturer) were respectively used as blank and positive control for the assay. Next, samples were transferred to 96-well Rho-GTP binding plates (Part #GL25), equipped with pre-washed GLISA assay strips, incubated at 4 °C, on an orbital microplate shaker at 400 rpm, for 30 min. Samples were then washed with wash buffer (Part # GL38) and incubated with Antigen Presenting Buffer (Part#GL45) for 2 min, washed again with wash buffer, then incubated at room temperature for 45 min, on orbital microplate shaker at 400 rpm, with anti-RhoA primary antibody (Part # GL01) (1:250) in Antigen dilution buffer (Part #GL40) and washed subsequently. Samples were next incubated with (1:62.5) secondary horseradish peroxidase (HRP) conjugate antibody (Part #GL02) at room temperature, for 45 min, on an orbital microplate shaker at 400 rpm, and washed afterwards. Then samples were incubated with HRP detection reagents A (Part # GL43) and B (Part # GL44) (1:1 ratio) for 15 min, at 37 °C, and reaction was stopped by adding HRP Stop Buffer (Part #GL80), and absorbance measured at 490 nm using a microplate spectrophotometer. To measure RhoA activity, values were determined as follows:  $(\frac{\text{GLISA value}(\text{ng})}{\text{ELISA value}(\text{ng})} \times 100 = \text{normalized \% of active RhoA})$ . The detected signal was normalized against total RhoA using G-LISA and E-LISA (BK#150) kits side by side. To determine if any significant difference existed in the activity of RhoA among samples, two-way ANOVA was performed in the grouped data followed by Bonferroni's post-hoc test. Results were presented as average of at least three independent experiments.

### Brain sectioning

Brains were collected from the Wt-PFTK1 and KO-PFTK1 mice at 8 weeks of age. Animals were humanely anesthetized with euthasol and transcardially perfused with 0.9% saline, followed by fixative solution 4% Paraformaldehyde (PFA) (EMD, PX0055-3) in 1×PBS at pH=7.4. Brains were then removed from the skull and fixed further with 4% PFA, at 4 °C, for 24 h. Fixed brain tissue was cryopreserved in 20% sucrose in 0.1 M phosphate buffer and stored at 4 °C, over a 3-day course, and the solution was changed 3 times per day. Brains were then snap-frozen with nitrogen balanced with CO<sub>2</sub> and then embedded with O.C.T. (Tissue—Tek /O.C.T compound, 4583) for sectioning. 14-μm coronal sections were collected from the brains, starting at the frontal cortex at Bregma: ~2.710 mm up to the 4th ventricle at Bregma: ~ -4.20 mm. For collecting, 3 sections were skipped in between each selection. Sections were directly mounted onto SuperFrost Plus microscopic slides 25×75×1.0 mm (Fisher brand, 12-550-15) and subjected to 2% cresyl violet staining as described below.

### Cresyl violet staining

Sections were thawed on a slide warmer for 15–20 min, at 35 °C, and then placed in distilled water for 5 min. Sections were then stained with 2% filtered cresyl violet (pH=3.5) cresyl violet acetate (C18H15N3O3, Sigma C5042-10G), for 10–30 min depending on the stain concentration. Sections were then dehydrated in graded ethanol solutions from 50 to 100%, followed by defatting with xylene. Sections were mounted with coverslips using toluene.

### Immunostaining

Cells plated on glass coverslips were fixed in 4% PFA in 1×PBS, for 15 min. Fixed cells were permeabilized and blocked simultaneously in 0.1% Triton X-100, and 5% BSA in 1×PBS, respectively, for 20 min, at room temperature. Coverslips were incubated with primary antibodies diluted in 5% BSA in 1×PBS: Tau1 clone 46 (1:500) mouse monoclonal IgG (Sigma-Aldrich, T-9450), GFP (H-140) (1:500) mouse monoclonal IgG (Abcam, ab1218), PFTK1 (H-140) (1:500) rabbit polyclonal IgG (SantaCruz, sc-50475), MAP2 (H-300) (1:500) rabbit polyclonal IgG (SantaCruz, sc-20172) for 1 h, at room temperature. Coverslips were washed, incubated with FITC-secondary antibodies: Alexafluor 488 (1:1000) Goat-Anti-mouse (Molecular Probes, A11001), Streptavidin Alexafluor 488 (1:1000) Goat-Anti-mouse (Molecular Probes, S11223), Streptavidin Alexafluor 546 (1:1000) Goat-Anti-mouse (Molecular Probes, S11225), Alexafluor 594 (1:1000) Goat-Anti-mouse (Molecular Probes, A11005), Alexafluor 594 (1:1000) Goat-Anti-rabbit (Molecular Probes, A11037), Alexafluor 594 (1:1000) Donkey-Anti-Goat (Molecular Probes, A11058) which were diluted in 5% BSA in 1×PBS and then incubated with coverslips for 30 min, at room temperature. To detect intact nuclei, cells were stained with Hoechst 33,258 (1:10,000) (Sigma-Aldrich B2883) in 1- PBS, incubated for a minimum of 30 min, at room temperature. Slides were immersed in distilled water to remove excess salt and then mounted on slides applying approximately 25 μl of Vectashield Mounting Medium (Vector laboratories, H-1200).

### Microscopy and imaging

Images were taken using upright Zeiss Axioskop 2 Mot or invert Zeiss AxioObserver-Z1 fluorescent microscope with Northern Eclipse Software or Zeiss and Axiovision Rel. 4.8 software, captured in XY mosaic format, in rectangle mode. Images were taken at 20×, 32×, and 40× magnification lenses. To determine the total diameter of the field of view for each objective, the ocular field of view (F.O.V.) number (32) was divided by objective magnification and the following measurements were

obtained: for 20×(1500 μm), for 32×(719 μm), and for 40×(575 μm). Images were processed for length measurements using Axiovision software Rel. 4.8, spline mode to trace axon length or Stereo Investigator microscopy imaging system (version 6; MicroBrightField, Williston, VT) software using contour mapping mode and tracing the length of axons. The distance from the cell body of the GFP-expressing neuron or Tau1 to the distal region of the longest neurite was measured as axon/lengthiest neurite.

### Quantification of signal density on images

Immunoblots were further analyzed by Image J software to compare the density/intensity of the bands of an agar gel or a western blot membrane. Following imaging of the blots, representative bands were selected, and their intensity was quantified. Then quantified measurements were transferred to Excel and results were normalized against relative controls (β-actin for Western blot and S12 for RT-PCR).

### Abbreviations

CDK	Cyclin-dependent kinases
Eip63E	Ecdysone-induced protein 63E
PFTK1	PFTAIRE kinase 1
TRAIL	Tumor necrosis factor-related apoptosis-inducing ligand
mRNA	Messenger ribonucleic acid
GFP	Green fluorescence protein
Sim	Single-minded
HRP	Horseradish peroxidase
RhoA	Ras homolog family member A
VNC	Ventral nerve cord
KO	Knockout
WT	Wildtype
ELAV	Embryonic lethal abnormal visual
KD	Knockdown
CNS	Central nervous system
PNS	Peripheral nervous system
Dmel	<i>Drosophila melanogaster</i>
RBD	Rho-binding domain

### Supplementary Information

The online version contains supplementary material available at <https://doi.org/10.1186/s12915-023-01732-w>.

**Additional file 1: Fig. S1.** Eip63E deficiency leads to concerted defects in axons and neurons of the *Drosophila* VNC. The combined penetrance of markers relevant to the same VNC structures are presented as one. Axon-associated penetrance reflects those calculated using HRP, BP-102 and Fasciclin-II antibodies. Neuron-related values include Neuroglian, Elav and Futsch-revealed penetrance. Penetrance was calculated as the % of defective embryos from the total embryos screened. Both deficient lines show the same nature of defects. Although it seems that defects associated to the Df(3L)E1 allele are more acute and appear later in development, Eip63E81 shows a robust axonal phenotype. ND: Not determined. **Fig. S2.** Eip63E functionally interacts with Rac1 and Cdc42 in *D. melanogaster* to regulate axogenesis. Ventral views of stage 14-15 whole mount embryos stained for BP102 antigen are shown head to the left. Panels show representative images for each specified genotype. An UAS-elavGal4 approach was used to drive Eip63E downregulation and either constitutively active or dominant negative forms of Rac1 or Cdc42 overexpression in neurons

of independent *D. mel.* lines. Fly genotype following crosses are indicated. (A-F) Neuronal functional interaction between Eip63E and Rac1. Only the combination of Eip63E deficiency and constitutively active Rac1 (UAS Rac1 V12; D), but not DN-Rac1 (UAS Rac1 N17; F), leads to an intermediate phenotype. (G-L) Functional interaction between Eip63E and Cdc42. Ventral views of the indicated genotypes of crosses between Eip63E and Cdc42 constitutive active form (UAS Cdc42 V12) or the dominant negative Cdc42 (UAS Cdc42 N17) are presented. Scale bar 50 μm. **Fig. S3.** Strategy for generation of PFTK1 KO murine line. The mouse was designed and developed by the Texas A&M Institute for Genomic Medicine (TIGM) (A) Strategy. Exon 6 (from nucleotide 18-Exon6 to nucleotide 1-Exon7) of the Cdk.14 gene at chromosomes (4,803,391-5,380,19 7) was replaced for an IRES/bGeo/Poly A cassette by homologous recombination. (B) Southern Blot screening of clones. (C). PCR strategy for genotyping. Bottom panel shows representative gel image with samples from the three possible genotypes. **Fig. S4.** PFTK1 deficiency does not appear to cause any gross brain defects or lethality. (A) Brains from three-month-old mice (3rd generation backcrossed) were collected, perfused, and fixed for sectioning. 14μm sections were collected from cryopreserved samples, starting from the cortex at bregma: ~ 2.710 mm up through the 4th ventricle at bregma: ~ -4.20 mm. Sections were then stained with cresyl violet to examine the gross anatomy of the brain. No abnormality was detected for KO mice (n=3/genotype). Representative sections from bregma 1.98, 1.70, 0.74, 1.00, 1.64, and 2.75 mm are presented. (B). Embryos or mice (=> 6th generation backcrossed) from HET x HET crosses were genotyped and incidence of the three possible outcomes is presented as % of the total n. No gross deviation from the expected 25:50:25 Mendelian ratio was detected. Scale bar 1 mm. **Fig. S5.** Differential expression of Rho GTPases in brains of Wt vs KO E13-14 murine embryos. Only RhoA is dysregulated in cortical neurons. Basal levels of RhoA and Rac1 protein in WT and Pftk1-deficient cortical neurons. Primary cortical neurons from E13-14 embryos from HET x HET crosses were dissected and plated at 0.65-0.75x10<sup>6</sup> cells/ml. After 18-20h in vitro, proteins were extracted followed by western blot. Top: Representative images from western blot are shown. Bottom, levels were assessed by densitometry using Image J and Rho GTPases signals were standardized vs loading control (Actin). Each column represents the average from 3 embryos/genotype +SEM. Significant difference between WT and KO neurons was only found for RhoA levels. Each column represents the average from n embryos/genotype +SEM. t-test was used for statistical analysis whenever a p value is specified. **Fig. S6.** Manipulation of PFTK1 levels has no impact on neuronal survival. Primary cortical neurons derived from CD1 embryos (E 14-15) were infected with 100 MOI of adenoviruses expressing GFP alone, GFP and WT- PFTK1 or GFP and D228N- PFTK1. After 12 or 24 hours in culture, cells were fixed and stained with Hoechst 33258 (nuclei visualization). nuclear integrity of GFP+ neurons was used as a criterion for vitality. Survival values represent the % of healthy nuclei of the total GFP+ cells. Table is showing average +SEM from three independent experiments. Graph shows the same data but presented as value relative to the GFP control.

**Additional file 2.** Uncropped blots.

### Acknowledgements

We are grateful for the contributions of Dr. Fatemeh Kamkar who passed away during the preparation of the manuscript.

### Authors' contributions

All authors read and approved the final manuscript. YRG and DSP conceived the project. YRG and FK designed the experiments. YRG, FK, PJ, DQ, and DH performed the experiments. PRA designed, cloned, and supplied the PFTAIRE constructs. LSA produced the adenoviruses. YRG and AJ wrote and technically edited the manuscript. RS provided scientific guidance and materials for experiments. DSP and AJ are responsible for general supervision of research and administrative support.

### Funding

This work was supported by grants from the Canadian Institutes of Health Research (grant numbers FRN # 15123 and 148402), Heart and Stroke Foundation of Ontario (HSFO), Canadian Stroke Network, and Centre for Stroke Recovery, Parkinson Society Canada, Parkinson's Disease Foundation, Parkinson's

Research Consortium, and Michael J. Fox Foundation (DSP). YRG. was supported by grants from Ontario Graduate Scholarship in Science and Technology and Ontario Graduate Scholarship. DSP is an HSFO Career Investigator.

#### Availability of data and materials

All data generated or analyzed during this study are included in this published article and its supplementary information files. All other data supporting the findings of this study are available from the corresponding author upon reasonable request.

#### Declarations

##### Ethics approval and consent to participate

Not applicable.

##### Consent for publication

Not applicable.

##### Competing interests

PJ is a paid employee of Ionis Pharmaceuticals Inc. The other authors declare that they have no competing interests.

Received: 26 September 2022 Accepted: 11 October 2023

Published online: 31 October 2023

#### References

- Malumbres M, Barbacid M. Mammalian cyclin-dependent kinases. *Trends Biochem Sci.* 2005;30(11):630–41.
- Jiang M, Gao Y, Yang T, Zhu X, Chen J, Cyclin Y. A novel membrane-associated cyclin, interacts with PFTK1. *FEBS Lett.* 2009;583(13):2171–8.
- Mikolcovic PSR, Rauch V, Hess MW, Pfaller K, Barisic M, Pelliniemi LJ, Boels M, Geley S Cyclin-dependent kinase 16 /PCTAIRE kinase 1 is activated by cyclin Y and is essential for spermatogenesis. *Mol Cell Biol.* 2012;32(4):868–79.
- Sauer K, Weigmann K, Sigrist S, Lehner CF. Novel members of the cdc2-related kinase family in *Drosophila*: cdk4/6, cdk5, PFTAIRE, and PITSLRE kinase. *Mol Biol Cell.* 1996;7(11):1759–69.
- Lazzaro MA, Julien JP. Chromosomal mapping of the PFTAIRE gene, Pftk1, a cdc2-related kinase expressed predominantly in the mouse nervous system. *Genomics.* 1997;42(3):536–7.
- Yang T, Chen JY. Identification and cellular localization of human PFTAIRE1. *Gene.* 2001;267(2):165–72.
- Lazzaro MA, Albert PR, Julien JP. A novel cdc2-related protein kinase expressed in the nervous system. *J Neurochem.* 1997;69(1):348–64.
- Besset V, Rhee K, Wolgemuth DJ. The identification and characterization of expression of Pftaire-1, a novel Cdk family member, suggest its function in the mouse testis and nervous system. *Mol Reprod Dev.* 1998;50(1):18–29.
- Stowers RS, Garza D, Rasclé A, Hogness DS. The L63 gene is necessary for the ecdysone-induced 63E late puff and encodes CDK proteins required for *Drosophila* development. *Dev Biol.* 2000;221(1):23–40.
- Liu J, Kipreos ET. Evolution of cyclin-dependent kinases (CDKs) and CDK-activating kinases (CAKs): differential conservation of CAKs in yeast and metazoa. *Mol Biol Evol.* 2000;17(7):1061–74.
- Park MH, Kim SY, Kim YJ, Chung Y-H. ALS2CR7 (CDK15) attenuates TRAIL induced apoptosis by inducing phosphorylation of survivin Thr34. *2014;450(1):129–34.*
- Garbe DS, Bashaw GJ. Axon guidance at the midline: from mutants to mechanisms. *Crit Rev Biochem Mol Biol.* 2004;39(5–6):319–41.
- Sanchez-Soriano N, Tear G, Whittington P, Prokop A. *Drosophila* as a genetic and cellular model for studies on axonal growth. *Neural Develop.* 2007;2:9.
- Cook HA, Koppetsch BS, Wu J, Theurkauf WE. The *Drosophila* SDE3 homolog armitage is required for oskar mRNA silencing and embryonic axis specification. *Cell.* 2004;116(6):817–29.
- Casso D, Ramirez-Weber F, Kornberg TB. GFP-tagged balancer chromosomes for *Drosophila melanogaster*. *Mech Dev.* 2000;91(1–2):451–4.
- Fambrough D, Pan D, Rubin GM, Goodman CS, inventorsThe cell surface metalloprotease/disintegrin Kuzbanian is required for axonal extension in *Drosophila*. 1996.
- Hummel T, Schimmelpfeng K, Klambt C. Commissure formation in the embryonic CNS of *Drosophila*. *Development.* 1999;126(4):771–9.
- Klambt C, Jacobs JR, Goodman CS. The midline of the *Drosophila* central nervous system: a model for the genetic analysis of cell fate, cell migration, and growth cone guidance. *Cell.* 1991;64(4):801–15.
- Nambu JR, Franks RG, Hu S, Crews ST. The single-minded gene of *Drosophila* is required for the expression of genes important for the development of CNS midline cells. *Cell.* 1990;63(1):63–75.
- Weigmann K, Klapper R, Strasser T, Rickert C, Technau G, Jäckle H, et al. FlyMove – a new way to look at development of *Drosophila*. *Trends Genet.* 2003;19:310.
- Bhat KM, Schedl P. Requirement for engrailed and invected genes reveals novel regulatory interactions between engrailed/invected, patched, gooseberry and wingless during *Drosophila* neurogenesis. *Development.* 1997;124(9):1675–88.
- Bhat KM. Segment polarity genes in neuroblast formation and identity specification during *Drosophila* neurogenesis. *BioEssays.* 1999;21(6):472–85.
- Jacobs JR, Goodman CS. Embryonic development of axon pathways in the *Drosophila* CNS. II. Behavior of pioneer growth cones. *J Neurosci.* 1989;9(7):2412–22.
- Snow PM, Patel NH, Harrelson AL, Goodman CS. Neural-specific carbohydrate moiety shared by many surface glycoproteins in *Drosophila* and grasshopper embryos. *J Neurosci.* 1987;7(12):4137–44.
- Desai CJ, Popova E, Zinn K. A *Drosophila* receptor tyrosine phosphatase expressed in the embryonic CNS and larval optic lobes is a member of the set of proteins bearing the “HRP” carbohydrate epitope. *J Neurosci.* 1994;14(12):7272–83.
- Robinow S, White K. Characterization and spatial distribution of the ELAV protein during *Drosophila melanogaster* development. *J Neurobiol.* 1991;22(5):443–61.
- Jimenez F, Campos-Ortega JA. Genes in subdivision 1B of the *Drosophila melanogaster* X-chromosome and their influence on neural development. *J Neurogenet.* 1987;4(4):179–200.
- Hortsch M, Bieber AJ, Patel NH, Goodman CS. Differential splicing generates a nervous system-specific form of *Drosophila* neuroglian. *Neuron.* 1990;4(5):697–709.
- Hummel T, Kruckert K, Roos J, Davis G, Klambt C. *Drosophila* Futsch/22C10 is a MAP1B-like protein required for dendritic and axonal development. *Neuron.* 2000;26(2):357–70.
- Chotard C, Salecker I. Neurons and glia: team players in axon guidance. *Trends Neurosci.* 2004;27(11):655–61.
- Freeman MR. Sculpting the nervous system: glial control of neuronal development. *Curr Opin Neurobiol.* 2006;16(1):119–25.
- Parker RJ, Auld VJ. Signaling in glial development: differentiation migration and axon guidance. *Biochem Cell Biol.* 2004;82(6):694–707.
- Xiong WC, Okano H, Patel NH, Blendy JA, Montell C. repo encodes a glial-specific homeo domain protein required in the *Drosophila* nervous system. *Genes Dev.* 1994;8(8):981–94.
- Duffy JB. GAL4 system in *Drosophila*: a fly geneticist's Swiss army knife. *Genesis.* 2002;34(1–2):1–15.
- Reichhart JM, Ferrandon D. Green balancers *Drosophila* Information Service. 1998;81:201–2.
- Nikolic MCM, Lu W, Mayer BJ, Tsai LH. The p35/Cdk5 kinase is a neuron-specific Rac effector that inhibits Pak1 activity. *Nature.* 1998;395:194–8.
- Rashid TBM, Nikolic M. Phosphorylation of Pak1 by the p35/Cdk5 kinase affects neuronal morphology. *J Biol Chem.* 2001;276:49043–52.
- Matsuda S, Kominato K, Koide-Yoshida S, Miyamoto K, Isshiki K, Tsuji A, et al. PCTAIRE kinase 3/cyclin-dependent kinase 18 is activated through association with cyclin A and/or phosphorylation by protein kinase A. *J Biol Chem.* 2014;289(26):18387–400.
- Warner SJ, Longmore GD. Distinct functions for Rho1 in maintaining adherens junctions and apical tension in remodeling epithelia. *J Cell Biol.* 2009;185(6):1111–25.

40. Nikolic MDH, Kwon YT, Ramos YF, Tsai LH. The cdk5/p35 kinase is essential for neurite outgrowth during neuronal differentiation. *Genes Dev.* 1996;10(7):816–25.
41. Cole AR. PCK Proteins: The Forgotten Brain Kinases? *Neurosignals.* 2009;17:288–97.
42. Flatau G, Lemichez E, Gauthier M, Chardin P, Paris S, Fiorentini C, et al. Toxin-induced activation of the G protein p21 Rho by deamidation of glutamine. *Nature.* 1997;387(6634):729–33.
43. Kranenburg O, Poland M, Gebbink M, Oomen L, Moolenaar WH. Dissociation of LPA-induced cytoskeletal contraction from stress fiber formation by differential localization of RhoA. *J Cell Sci.* 1997;110(Pt 19):2417–27.
44. Tong J, Li L, Ballermann B, Wang Z. Phosphorylation and activation of RhoA by ERK in response to epidermal growth factor stimulation. *PLoS ONE.* 2016;11(1): e0147103.
45. Forget M-A, Desrosiers RR, Gingras D, Béliveau R. Phosphorylation states of Cdc42 and RhoA regulate their interactions with Rho GDP dissociation inhibitor and their extraction from biological membranes. *Biochemical Journal.* 2002;361(2):243.
46. Ellerbroek SM, Wennerberg K, Burridge K. Serine phosphorylation negatively regulates RhoA in vivo. *J Biol Chem.* 2003;278(21):19023–31.
47. Isshiki T, Pearson B, Holbrook S, Doe CQ. *Drosophila* neuroblasts sequentially express transcription factors which specify the temporal identity of their neuronal progeny. *Cell.* 2001;106(4):511–21.
48. Grosskortenhaus R, Pearson BJ, Marusich A, Doe CQ. Regulation of temporal identity transitions in *Drosophila* neuroblasts. *Dev Cell.* 2005;8(2):193–202.
49. Bettencourt-Dias M, Giet R, Sinka R, Mazumdar A, Lock WG, Balloux F, et al. Genome-wide survey of protein kinases required for cell cycle progression. *Nature.* 2004;432(7020):980–7.
50. Davidson G, Shen J, Huang YL, Su Y, Karaulanov E, Bartscherer K, et al. Cell cycle control of wnt receptor activation. *Dev Cell.* 2009;17(6):788–99.
51. Zechner D, Fujita Y, Hulsken J, Muller T, Walther I, Takeo MM, et al. beta-Catenin signals regulate cell growth and the balance between progenitor cell expansion and differentiation in the nervous system. *Dev Biol.* 2003;258(2):406–18.
52. Grigoryan T, Wend P, Klaus A, Birchmeier W. Deciphering the function of canonical Wnt signals in development and disease: conditional loss- and gain-of-function mutations of beta-catenin in mice. *Genes Dev.* 2008;22(17):2308–41.
53. Sanchez-Soriano N, Prokop A. The influence of pioneer neurons on a growing motor nerve in *Drosophila* requires the neural cell adhesion molecule homolog FasciclinII. *J Neurosci.* 2005;25(1):78–87.
54. Yao KM, White K. Neural specificity of elav expression: defining a *Drosophila* promoter for directing expression to the nervous system. *J Neurochem.* 1994;63(1):41–51.
55. Hodge RG, Ridley AJ. Regulating Rho GTPases and their regulators. *Nat Rev Mol Cell Biol.* 2016;17(8):496–510.
56. Heasman SJ, Ridley AJ. Mammalian Rho GTPases: new insights into their functions from in vivo studies. *Nat Rev Mol Cell Biol.* 2008;9(9):690–701.
57. Garcia-Mata R, Boulter E, Burridge K. The 'invisible hand': regulation of RHO GTPases by RHOGDIs. *Nat Rev Mol Cell Biol.* 2011;12(8):493–504.
58. Jin Z, Strittmatter SM. Rac1 mediates collapsin-1-induced growth cone collapse. *J Neurosci.* 1997;17(16):6256–63.
59. Kozma R, Sarner S, Ahmed S, Lim L. Rho family GTPases and neuronal growth cone remodelling: relationship between increased complexity induced by Cdc42Hs, Rac1, and acetylcholine and collapse induced by RhoA and lysophosphatidic acid. *Mol Cell Biol.* 1997;17(3):1201–11.
60. Kuhn TB, Brown MD, Wilcox CL, Raper JA, Bamberg JR. Myelin and collapsin-1 induce motor neuron growth cone collapse through different pathways: inhibition of collapse by opposing mutants of rac1. *J Neurosci.* 1999;19(6):1965–75.
61. Zipkin ID, Kindt RM, Kenyon CJ. Role of a new Rho family member in cell migration and axon guidance in *C. elegans*. *Cell.* 1997;90(5):883–94.
62. Threadgill R, Bobb K, Ghosh A. Regulation of dendritic growth and remodeling by Rho, Rac, and Cdc42. *Neuron.* 1997;19(3):625–34.
63. Okuda T CJ, Downing JR. PCTAIRE-1 and PCTAIRE-3, two members of a novel cdc2/CDC28-related protein kinase gene family. *Oncogene.* 1992;7(11).
64. Hirose TKM, Tamaru T, Okumura N, Nagai K, Okada M. Identification of tudor repeat associator with PCTAIRE 2 (Trap). A novel protein that interacts with the N-terminal domain of PCTAIRE 2 in rat brain. *Eur J Biochem.* 2000;267(7):2113–21.
65. Chen Y, Yang Z, Meng M, Zhao Y, Dong N, Yan H, et al. Cullin mediates degradation of RhoA through evolutionarily conserved BTB adaptors to control actin cytoskeleton structure and cell movement. *Mol Cell.* 2009;35(6):841–55.
66. Sebok ANN, Debrececi B, Guo Z, Santos MF, Szeberenyi J, Tigyi G. Different roles for RhoA during neurite initiation, elongation, and regeneration in PC12 cells. *J Neurochem.* 1999;73(3):949–60.
67. Chang F, Lemmon C, Lietha D, Eck M, Romer L. Tyrosine phosphorylation of Rac1: a role in regulation of cell spreading. *PLoS ONE.* 2011;6(12): e28587.
68. Ashburner M. *Drosophila: a laboratory manual.* Harbor CS, editor: Cold Spring Harbor Press; 1989. 402.
69. Campos-Ortega J, Hartenstein V. *The embryonic development of Drosophila melanogaster.* Berlin: Springer Verlag; 1985.
70. Harlow E, Lane D. *Preparing early whole-mount Drosophila embryos for immunostaining: Cold Spring Harbor Protocols.* doi:<https://doi.org/10.1101/pdb.prot4524>; 2006. 23.
71. Benveniste RJ, Thor S, Thomas JB, Taghert PH. Cell type-specific regulation of the *Drosophila* FMRF-NH2 neuropeptide gene by Apterous, a LIM homeodomain transcription factor. *Development.* 1998;125(23):4757–65.
72. Lazzaro MAAP, Julien JP. A novel cdc2-related protein kinase expressed in the nervous system. *J Neurochem.* 1997;69(1):348–64.

## Publisher's Note

Springer Nature remains neutral with regard to jurisdictional claims in published maps and institutional affiliations.

Ready to submit your research? Choose BMC and benefit from:

- fast, convenient online submission
- thorough peer review by experienced researchers in your field
- rapid publication on acceptance
- support for research data, including large and complex data types
- gold Open Access which fosters wider collaboration and increased citations
- maximum visibility for your research: over 100M website views per year

At BMC, research is always in progress.

Learn more [biomedcentral.com/submissions](https://biomedcentral.com/submissions)

